The effect of atmosphere-ocean coupling on the sensitivity of the ITCZ to convective mixing

JAMES | Journal of Advances in Modeling Earth Systems

RESEARCH ARTICLE
10.1029/2020MS002322

The Effect of Atmosphere-Ocean Coupling on the Sensitivity of the ITCZ to Convective Mixing

J. Talib[1,2], S. J. Woolnough[3], N. P. Klingaman[3], and C. E. Holloway[1]

[1]Department of Meteorology, University of Reading, Reading, UK, [2]UK Centre for Ecology and Hydrology, Wallingford, UK, [3]National Centre for Atmospheric Science-Climate, Reading, UK

Key Points:
- Atmosphere-ocean coupling reduces the sensitivity of the simulated ITCZ to convective mixing
- Sea surface temperature variations are predominately responsible for the reduced sensitivity
- Atmospheric energy input framework to understand ITCZ behavior has significant limitations due to strong transient eddies

Correspondence to:
J. Talib,
jostal@ceh.ac.uk

Citation:
Talib, J., Woolnough, S. J., Klingaman, N. P., & Holloway, C. E. (2020). The effect of atmosphere-ocean coupling on the sensitivity of the ITCZ to convective mixing. *Journal of Advances in Modeling Earth Systems*, *12*, e2020MS002322. https://doi.org/10.1029/2020MS002322

Received 27 AUG 2020
Accepted 9 NOV 2020
Accepted article online 13 NOV 2020

Abstract The Intertropical Convergence Zone (ITCZ) is a discontinuous, zonal precipitation band that plays a crucial role in the global hydrological cycle. Previous studies using prescribed sea surface temperature (SST) aquaplanets show the ITCZ is sensitive to convective mixing, but such a framework is energetically inconsistent. Studies also show that atmosphere-ocean coupling reduces the sensitivity of the ITCZ to hemispherically asymmetric forcing. We investigate the effect of atmosphere-ocean coupling on the sensitivity of the ITCZ to convective mixing using an idealized modeling framework with an Ekman-driven ocean energy transport (OET). Coupling reduces the sensitivity of the ITCZ location to convective mixing due to SST changes. In prescribed-SST simulations reducing convective mixing promotes a double ITCZ, while in coupled simulations, it increases the meridional SST gradient which promotes an equatorward ITCZ shift. Prescribing OET in additional experiments has a minimal effect on the sensitivity of the ITCZ location to mixing but does increase the sensitivity of the ITCZ intensity by constraining the net-downward surface energy flux. Decreasing convective mixing increases net-downward shortwave cloudy-sky radiation associated with increased latent heat fluxes and an intensified ITCZ. For simulations analyzed the atmospheric energy input framework is inadequate to study ITCZ dynamics due to the contribution of transient eddies to the atmospheric energy transport. Prescribing SST or OET may strengthen the sensitivity of the ITCZ to a change in parameterization or atmospheric forcing. Future modeling studies investigating the precipitation response to such changes should be aware of the potential sensitivity of their results to atmosphere-ocean interactions.

Plain Language Summary The Intertropical Convergence Zone (ITCZ) is a discontinuous tropical rainfall band with over three billion livelihoods dependent on its seasonal cycle. However, even the latest state-of-the-art climate models poorly simulate the real-world ITCZ. Previous modeling studies which fix sea surface temperatures and have no land show that the ITCZ is sensitive to the model's representation of deep clouds. However, it is yet to be determined whether ocean dynamics that are influenced by the atmosphere removes this sensitivity.
In this study we couple the atmosphere to an ocean model with a circulation that depends on near-surface winds. Through doing so we highlight that interactions between the atmosphere and ocean reduce changes in ITCZ location when varying the representation of deep clouds. This is predominately associated with sea surface temperature changes rather than changes in ocean circulation. However, fixing the ocean circulation and only allowing sea surface temperatures to vary, can cause different changes in ITCZ intensity when changing the representation of deep clouds. We therefore highlight that fixing either sea surface temperatures or the ocean circulation can affect how the ITCZ responds to changes in model design.

1. Introduction

The Intertropical Convergence Zone (ITCZ) is a discontinuous zonal precipitation belt with some of the heaviest rainfall observed on Earth. Modeling tropical rainfall is one of the greatest challenges faced in climate science (Bush et al., 2015; Sperber et al., 2013). Most coupled general circulation models (GCMs) overestimate zonal-mean, time-mean tropical precipitation (De Szoeke & Xie, 2008; Lin, 2007). In the real world a single precipitation maximum is observed in the Northern Hemisphere along with a broader, weaker precipitation peak in the Southern Hemisphere. Meanwhile, the latest coupled GCMs simulate similar tropical precipitation maxima in each hemisphere (Lin, 2007; Tian & Dong, 2020). This bias is commonly known as the "double ITCZ bias"; it is associated with a positive precipitation bias in the South Pacific

Convergence Zone and a rainfall band in each hemisphere across the Central and East Pacific (Hwang & Frierson, 2013; Lin, 2007; Oueslati & Bellon, 2015; Tian & Dong, 2020). Atmospheric models are thought to be the dominant cause of the double ITCZ bias, as it remains in prescribed sea surface temperature (SST) atmosphere-only simulations (Lin, 2007). The bias in rainfall asymmetry in a coupled GCM can also be predicted from the hemispheric asymmetry in net-downward surface energy flux in the corresponding atmosphere-only configuration (Mobis & Stevens, 2012; Xiang et al., 2017).

1.1. Modeling Studies

The simulated ITCZ is sensitive to the representation of convection across a hierarchy of models (Bacmeister et al., 2006; Bush et al., 2015; Oueslati & Bellon, 2013; Song & Zhang, 2018; Zhang & Wang, 2006). In particular, the ITCZ is sensitive to convective mixing (Bush et al., 2015; Mobis & Stevens, 2012; Talib et al., 2018). Increased mixing reduces the systematic double ITCZ bias in both atmosphere-only and coupled GCMs (Chikira, 2010; Oueslati & Bellon, 2013; Terray, 1998). The double ITCZ bias in CMIP3 (Coupled Model Intercomparison Project Phase 3) simulations has been associated with weak convective mixing across subsidence regions (Hirota et al., 2011). However, increasing convective mixing can also lead to too much precipitation in convergence zones (Oueslati & Bellon, 2013; Song & Zhang, 2018), as mixing suppresses convection in drier environments and increases the moisture flux from subsidence regions into convergence zones (Bush et al., 2015; Klingaman & Woolnough, 2014; Oueslati & Bellon, 2013; Terray, 1998; Wang et al., 2007).

In full GCMs complex surface characteristics and boundary conditions including orography, land-sea contrasts, and SST gradients make it challenging to understand the sensitivity of the ITCZ to convective mixing (Bush et al., 2015; Oueslati & Bellon, 2013). Even in the absence of complex surface conditions, prescribed-SST aquaplanet simulations illustrate a sensitivity of the ITCZ to mixing (Mobis & Stevens, 2012; Oueslati & Bellon, 2013; Peatman et al., 2018; Talib et al., 2018). Increasing mixing reduces the moist static energy (MSE) difference between a convective plume, determined by the boundary layer MSE, and the free-troposphere. This increases the minimum boundary layer MSE required for deep convection thereby favoring a single rather than double ITCZ. In a prescribed-SST modelling framework, the requirement of greater boundary layer MSE for deep convection results in an equatorward contraction of the ITCZ (Talib et al., 2018).

However, prescribed-SST simulations are energetically inconsistent and prohibit atmosphere-ocean coupling, such that SSTs cannot respond to changes in surface forcing associated with ITCZ shifts. One solution to this problem, used by several studies, is to couple the atmosphere to a slab ocean with a prescribed ocean energy transport (OET) (Merlis et al., 2013; Schneider et al., 2014; Wei & Bordoni, 2018). However, while a slab ocean configuration with a prescribed OET is energetically consistent, it lacks a dynamic ocean response to changes in surface heat and momentum forcing. Previous studies show that the ocean circulation response to changes in atmospheric circulation reduces the sensitivity of the ITCZ to hemispherically asymmetric forcings (Green & Marshall, 2017; Hawcroft et al., 2017; Kang et al., 2018; Kay et al., 2016; Tomas et al., 2016). Atmosphere-ocean coupling also reduces the sensitivity of the ITCZ to convective mixing in the full GCM configuration of CNRM-CM5 (Oueslati & Bellon, 2013). Oueslati and Bellon (2013) propose that the reduced sensitivity is associated with coupled atmosphere-ocean feedbacks but do not hypothesize which processes are important. In this study we develop an idealized atmosphere-ocean coupled model, with an interactive OET based on the meridional Ekman-driven ocean circulation, to quantify the effect of atmosphere-ocean coupling on the sensitivity of the ITCZ to convective mixing. Previous studies that have coupled the atmosphere to an idealized ocean model that resolves the Ekman circulation simulate a double ITCZ associated with equatorial upwelling and a local equatorial SST minimum (Codron, 2012; Pike, 1971). This is the first aquaplanet study to investigate a sensitivity of the ITCZ to an atmospheric process or forcing in such a modeling framework. We hypothesize that coupling will substantially reduce the sensitivity of the ITCZ to convective mixing, as previous studies show that atmosphere-ocean coupling reduces the ITCZ response to hemispheric asymmetric forcing (Green & Marshall, 2017).

1.2. Atmospheric Energy Framework

Literature based on a hierarchy of models, as well as reanalyses and observations, concludes that ITCZ characteristics, including its location, structure, and width, are associated with meridional variations in

atmospheric energy input (AEI) and the associated atmospheric energy transport (AET) (Adam et al., 2016; Bischoff & Schneider, 2014, 2016; Byrne & Schneider, 2016b, Byrne et al., 2018; Donohoe et al., 2013; Frierson & Hwang, 2012; Kang, 2020; Kang et al., 2008). AEI is the net energy input to the atmosphere and is defined as

$$[\overline{AEI}] = [\overline{SW}]+[\overline{LW}]+[\overline{H}] \quad (1)$$

where [ ] and $^-$ denote the zonally averaged and time-averaged value respectively, SW and LW denote the net atmospheric heating from shortwave and longwave radiation respectively, and H denotes the atmospheric heating from surface sensible and latent heat fluxes. Bischoff and Schneider (2014) and Bischoff and Schneider (2016) developed a quantitative, diagnostic framework that relates the latitude of a single or double ITCZ to the cross-equatorial AET and equatorial AEI (AEI_0). A single ITCZ is associated with a positive AEI_0 and a double ITCZ is associated with a negative AEI_0 (Bischoff & Schneider, 2016). Stronger negative AEI_0 shifts a double ITCZ poleward. A key assumption in the AEI framework is that the meridional MSE flux is primarily controlled by the mean tropical circulation. It should also be noted that Bischoff and Schneider (2014) and Bischoff and Schneider (2016) only validate their framework in slab ocean simulations with a prescribed OET. In this study we investigate the validity of that assumption in our idealized simulations, particularly whether an AEI framework should be used to understand the sensitivity of the ITCZ structure to the representation of convection in a coupled atmosphere-ocean modeling configuration.

In this study, section 2 introduces the idealized atmosphere-ocean coupled modeling framework (section 2.1) and the simulations employed in this study (section 2.2). Section 3.1 describes the simulated characteristics of the tropical atmosphere and ocean when using the idealized coupled model. Section 3.2 discusses the sensitivity of the ITCZ to convective mixing in coupled simulations. Due to substantial mean-state changes when coupling, prescribed-SST simulations are performed with SSTs from interactive-OET simulations. Prescribed-SST simulations and prescribed-OET simulations are discussed in sections 3.3 and 3.4 respectively. Sections 4 and 5 end this study with discussion and conclusions.

2. Methodology

In this study the U.K. Met Office Unified Model (MetUM) Global Atmosphere 6.0 (GA6.0) at N96 resolution (1.25° latitude × 1.875° longitude) is coupled to an idealized two-layer ocean model. The atmospheric model is the same as in the prescribed-SST experiments in Talib et al. (2018). The idealized ocean model, similar to the "2-layer Ekman scheme" in Codron (2012), reproduces the structure of an Ekman-driven circulation, is computationally cheaper than coupling the atmosphere to a full dynamical ocean model, and is energetically consistent. It is also easier to understand the effect of the wind-driven circulation in the idealized modeling framework compared to fully coupled models, in which partitioning the effect of different ocean circulation components is nontrivial. In this section we introduce the design of the coupled modeling framework (section 2.1) and the experiments performed (section 2.2).

2.1. Coupled Atmosphere-Ocean Modeling Framework

A modeling framework is developed in which GA6.0 is coupled to an idealized zonally averaged axisymmetric two-layer ocean model with an Ekman-driven circulation. In the tropics the majority of meridional OET is associated with the Ekman-driven ocean circulation (Codron, 2012; Levitus, 1987). Surface frictional stress slows near-surface atmospheric winds, which leads to a poleward or equatorward near-surface Ekman mass flux for easterly or westerly winds, respectively (Schneider, 2018). The top layer of the two-layer ocean model (subscript m) represents the ocean mixed layer, while the bottom layer (subscript d) represents the deep ocean. The zonal-mean zonal surface wind stress (τ_x, kg m^{-1} s^{-2}) determines the zonally averaged meridional Ekman ocean current in the mixed layer (v_{ek_m}, m s^{-1}):

$$v_{ekm} = \frac{-[\tau_x]}{\rho f H_m} \quad (2)$$

where ρ is a fixed density (1030 kg m^{-3}), f is the Coriolis parameter (rad s^{-1}), [ ] represents the zonally averaged value, and H_m is a fixed ocean mixed layer depth (30 m). Within ±2.5° latitude of the equator, f at 2.5° latitude is prescribed to ensure that v_{ek_m} is not unrealistically large. Due to mass conservation

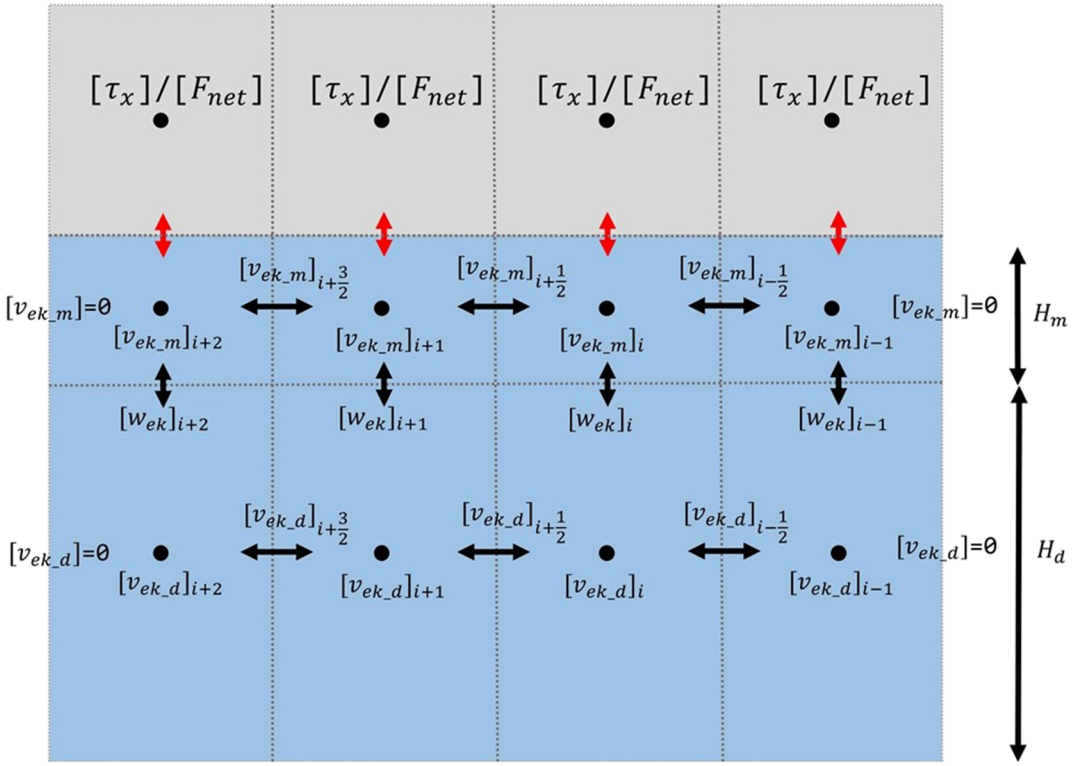

Figure 1. Schematic (not to scale) of the numerical scheme used for the two-layer ocean model. Grid points are denoted by filled circles. Ocean cell boundaries, where heat fluxes are computed, are denoted by black double-pointed arrows. The atmosphere-ocean boundary is denoted by double-pointed red arrows. H_m and H_d denote the mixed- and deep-layer depths, respectively.

the near-surface oceanic Ekman mass flux is associated with an overturning ocean circulation with a return flow at depth (Schott et al., 2004). Hence, the deep-layer mass flux (v_{ek_d}) is computed as follows:

$$v_{ekd} = -v_{ekm}\frac{H_m}{H_d} \tag{3}$$

where H_d is the depth of the deep ocean layer (970 m). The meridional Ekman-driven currents are calculated at the cell centers. Meridional Ekman currents at the cell boundaries are given using the average Ekman current at the two cell centers either side of the boundary (Figure 1):

$$v_{ek}^{i+\frac{1}{2}} = \frac{1}{2}(v_{ek}^{i+1} + v_{ek}^{i}) \tag{4}$$

where v_{ek_m} and v_{ek_d} are zero at the poles. The vertical zonally averaged Ekman-driven current (w_{ek}, m s^{-1}) is calculated using the meridional divergence (∂_y) of v_{ekm}:

$$w_{ek} = \partial_y(v_{ek\_m})H_m \tag{5}$$

All calculations are performed in spherical coordinates. The vertical and meridional Ekman currents are then multiplied by the up-current temperature to calculate the associated heat fluxes. The temperature tendencies at each grid point are calculated using the meridional divergence of the horizontal heat flux ($-\partial_y(v_{ek\_m}T_m)$, $-\partial_y(v_{ek\_d}T_d)$; later shown in 6 and 7) and the vertical heat flux divided by the layer depth ($\frac{w_{ek}T^*}{H_m}$, $\frac{w_{ek}T^*}{H_d}$; also shown in 6 and 7).

After developing a zonally averaged ocean model with an Ekman-driven circulation, it became evident that additional terms were required to maintain a realistic Earth-like ocean state. As a result, three additional components are imposed to the temperature tendencies of the mixed and deep ocean layers:

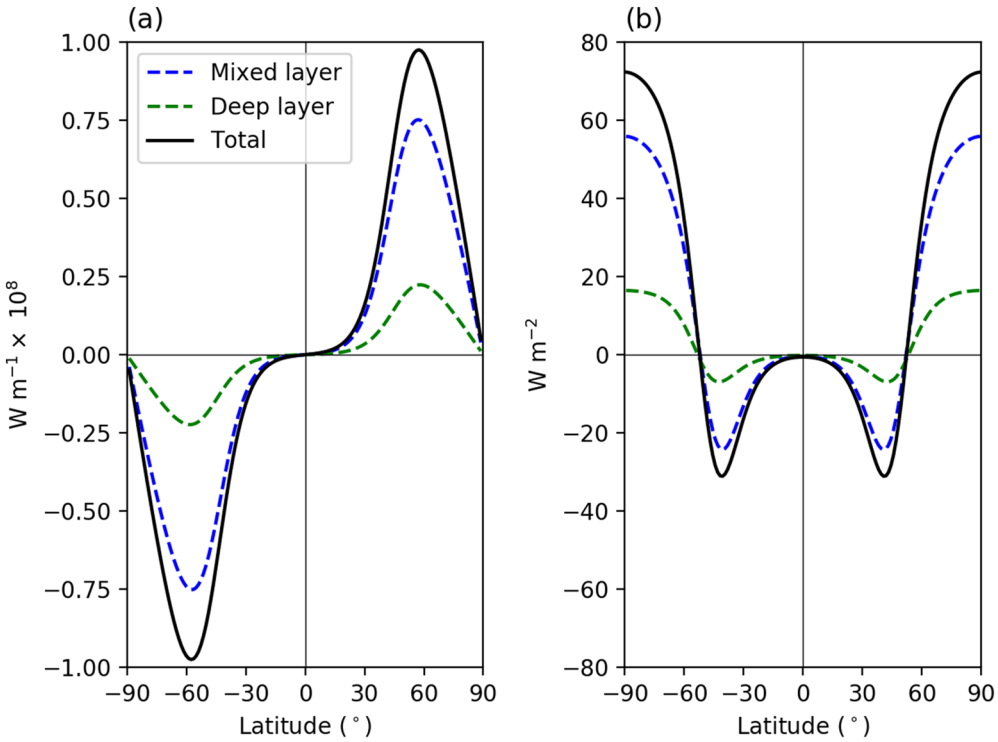

Figure 2. Prescribed (a) northward meridional ocean energy transport (*PHT*, W m^{-1}) and (b) extratropical q flux ($-1 \times \partial_y$ (*PHT*), W m^{-2}) in interactive-OET and prescribed-OET simulations (Table 1). Blue and green dashed lines denote mixed and deep ocean layers respectively. The black line denotes the sum of both layers.

- $\frac{\partial_y(PHT_m)}{\rho C_p H_m}$ and $\frac{\partial_y(PHT_d)}{\rho C_p H_d}$ - The divergence of a prescribed heat transport (PHT_m and PHT_d, W m^{-1}, Figure 2a) to maintain a realistic equator-to-pole temperature gradient and represent missing dynamical features such as barotropic gyres and large-scale density currents. C_p is a fixed specific heat capacity (4000 J kg^{-1} K^{-1}). The negative of the meridional divergence of *PHT* (Figure 2b, W m^{-2}), which is only substantial poleward of 25° latitude, is referred to as the "prescribed extratropical q flux" using similar terminology as Voigt et al. (2016). The prescribed extratropical q flux warms the high latitudes (> 50° latitude) and cools the subtropics (25° to 50°), while having a minimal effect in the deep tropics (< 25° latitude).
- $\frac{C^*(T_d - T_m)}{\rho C_p H_m}$ and $\frac{C^*(T_d - T_m)}{\rho C_p H_d}$ - Vertical mixing to represent either convective overturning or weak vertical diffusion. This is imposed because in initial experiments at high latitudes, SSTs cooled more rapidly than the deep ocean. If T^d is greater than T^m, then vertical mixing behaves like convection and rapidly reduces the vertical temperature gradient. If however T^m is greater than T^d, then mixing acts like vertical diffusion. A mixing coefficient (C^*, W K^{-1} m^{-2}), defined as 100.0 or 0.001 for upward (convection) or downward (diffusion) vertical mixing, respectively, is used to scale the heat transport associated with each process.
- $D\partial_{yy}T_d$ - A weak horizontal eddy diffusion in the deep ocean, where D is 1.0 m^2 s^{-1}, to remove any sharp horizontal temperature gradients.

The final temperature tendency equations for the mixed and deep ocean layers are

$$\frac{\partial T_m}{\partial t} = -\partial_y(v_{ekm}T_m) + \frac{w_{ek}T^*}{H_m} + \frac{1}{\rho C_p}\left[\frac{[F_{net}]}{H_m} - \frac{\partial_y(PHT_m)}{H_m} + \frac{C^*(T_d - T_m)}{H_m}\right] \quad (6)$$

$$\frac{\partial T_d}{\partial t} = -\partial_y(v_{ekd}T_d) - \frac{w_{ek}T^*}{H_d} - \frac{1}{\rho C_p}\left[\frac{\partial_y(PHT_d)}{H_d} - \frac{C^*(T_d - T_m)}{H_d}\right] + D\partial_{yy}T_d \quad (7)$$

Table 1
Interactive-OET Coupled Simulations

Simulation	f_{dp}	Ekman-driven q flux
C0.57	0.57	Interactive
C1.13	1.13	Interactive
C1.70	1.70	Interactive

where $[F_{net}]$ is the zonal-mean net-downward surface energy flux (W m^{-2}) and T^* the up-current temperature.

MetUM GA6.0 is coupled to the ocean using the Ocean Atmosphere Sea Ice Soil (OASIS) coupler (Valcke et al., 2013). Variables passed from the atmosphere to the ocean include surface energy and momentum flux components, and precipitation. T_m is passed to GA6.0 as the SST. The ocean model is run with an hourly time step.

To spin up the ocean model efficiently, "accelerated coupling" is used. Between atmosphere-ocean exchanges, the ocean model is integrated for thirty hours and the atmosphere is integrated for three hours. Accelerated coupling reduces computational cost by reducing the computational time required for the ocean to equilibrate, without affecting the conclusions in this study.

To achieve appropriate initial conditions for coupled experiments, we perform a spin-up simulation using accelerated coupling. The simulation uses the default MetUM GA6.0 configuration. It is initialized from an equilibrated prescribed-SST aquaplanet simulation with equatorial insolation and a "Qobs" SST profile (Neale & Hoskins, 2001a). After 10 years of atmospheric simulation (100 years of oceanic simulation), the tropical meridional SST structure and vertical temperature gradient remain similar with time (not shown). However, the global-mean ocean temperature continues to warm. The equilibrated model state is much warmer than observed SSTs with an average tropical SST of approximately 31°C. SSTs are most realistic to the real world after 15 years of atmospheric simulation. To achieve an Earth-like SST profile and restrict global-mean SST increases, we prescribe a spatially and temporally uniform surface energy flux correction of 4 W m^{-2} to all subsequent simulations which are initialized from the end of this 15 year spin-up simulation. Using a prescribed energy flux correction permits changes in SST in response to atmospheric physics changes, is energetically consistent, and produces a more realistic equilibrium SST profile.

2.2. Design of Interactive-OET Simulations

To explore the sensitivity of the ITCZ to convective mixing in an idealized atmosphere-ocean coupled modeling framework (section 2.1), we perform three coupled simulations varying the lateral entrainment (ϵ) and detrainment (d_m) rates for deep-level convection (Table 1) in the MetUM:

$$\epsilon = 4.5 f_{dp} \frac{p(z)\rho(z)g}{p_*^2} \tag{8}$$

$$d_m = 3.0(1 - RH)\epsilon \tag{9}$$

Both ϵ and d_m are given as a fractional mixing rate per unit length (m^{-1}). In 8 and 9, p and p_* are pressure and surface pressure (Pa); ρ is density (kg m^{-3}); g is gravitational acceleration (m s^{-2}); f_{dp} is a constant with a default value of 1.13; and RH is relative humidity. We control ϵ and d_m by scaling f_{dp} to 0.5, 1.0, and 1.5 times the default value: 0.57 (C0.57), 1.13 (C1.13), and 1.70 (C1.70). For each simulation 20 atmospheric years of accelerated coupling is followed by 10 atmospheric years of "normal" steady-state simulation. An equilibrated ocean state is achieved in all simulations during the first 20 years of accelerated coupling. The final 5 years of the steady-state simulation are analyzed unless stated otherwise. Coupled simulations with an interactive Ekman-driven q flux are referred to as "interactive-OET" simulations.

We also investigate the effect of atmosphere-ocean coupling on the sensitivity of the ITCZ to convective mixing by performing and analysing prescribed-SST and prescribed-OET simulations. These are discussed in more detail in sections 3.3 and 3.4 respectively.

3. Results

3.1. Climatology of Coupled Simulation

Before discussing the sensitivity of the ITCZ to convective mixing, we first describe the mean-state climate in an interactive-OET simulation where f_{dp} equals 1.13. C1.13 produces a double ITCZ associated with an equatorial local SST minimum and a negative AEI_0 of approximately −60 W m^{-2} (Figure 3). Easterly zonal wind stresses drive a poleward upper-ocean mass flux, leading to equatorial upwelling and an SST minimum.

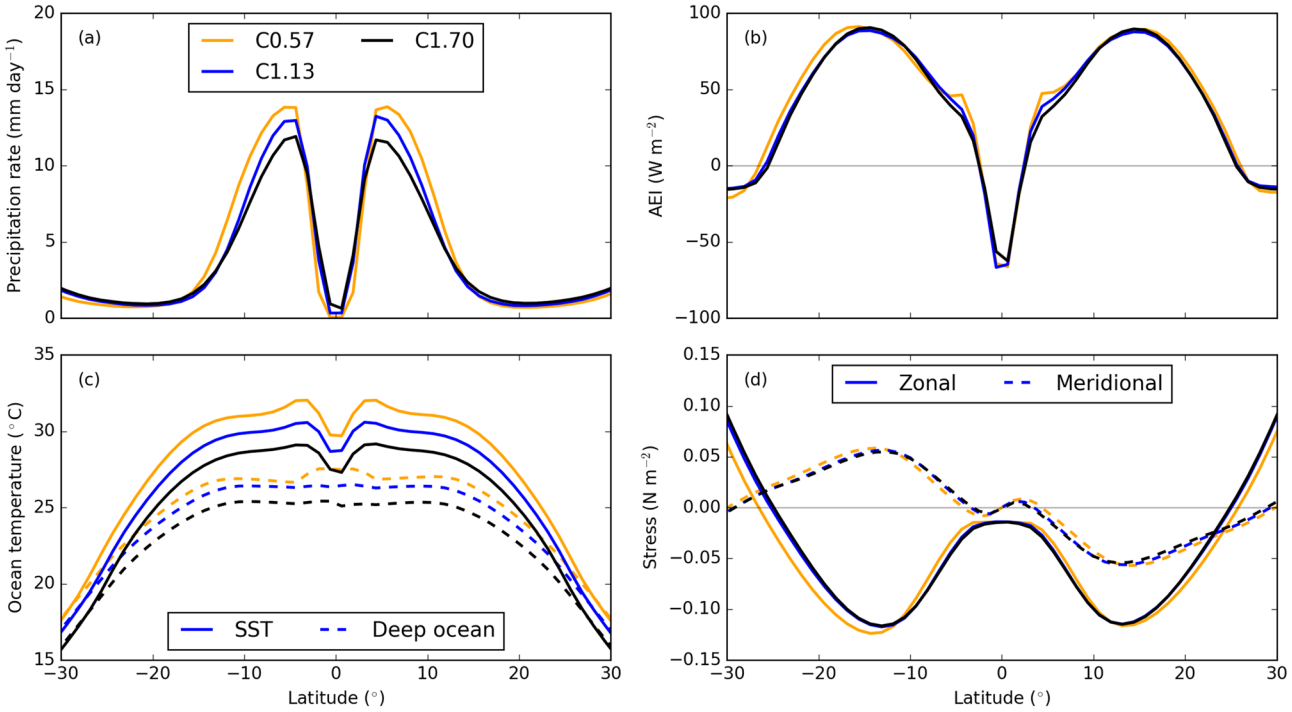

Figure 3. Zonal-mean, time-mean tropical (a) precipitation (mm day^{-1}); (b) AEI (W m^{-2}); (c) ocean temperatures (°C), where solid lines denote SSTs and dashed lines denote deep-layer ocean temperatures; and (d) zonal (solid) and meridional (dashed) surface wind stresses (N m^{-2}) in C0.57 (orange), C1.13 (blue), and C1.70 (black).

Cooler equatorial SSTs decrease the boundary layer MSE (Figure 4b), restricting equatorial convection and promoting a double ITCZ. Negative AEI_0 is associated with an equatorward AET across low latitudes (Figure 5a).

Figure 5 illustrates components of AET and OET in C1.13. By design the meridional tropical ocean energy flux is dominated by transport associated with the Ekman-driven circulation (Figure 5b). Further analysis reveals OET is primarily associated with the time-mean Ekman-driven circulation (not shown). Partitioning AET into mean and eddy components highlights that eddies dominate low-latitude equatorward AET (Figure 5a). While the mass meridional stream function shows equatorial subsidence throughout the troposphere (Figure 4b), the mean circulation plays a minimal role in low-latitude equatorward AET (Figure 5a). Partitioning the eddy-associated AET into dry static and latent energy components highlights equatorward AET is dominated by transient eddies transporting latent energy. From further analysis (not shown) these transient eddies are concluded to be westward propagating disturbances with a phase speed of approximately 4 to 8 m s^{-1}. The eddy-associated latent heat flux is substantial between 900 and 200 hPa, with a negligible flux in the boundary layer. The eddy-associated equatorial moisture convergence is balanced by moisture divergence by the mean circulation resulting in minimal equatorial precipitation. Eddies in C1.13 play a greater role in determining tropical AET than eddies in prescribed-SST simulations with a similar negative AEI_0 (Talib et al., 2018). The greater role for eddies in C1.13 is due to a strong equatorial SST minimum and substantial meridional moisture gradients.

The contribution of eddies to tropical AET in C1.13 reveals that the double ITCZ location cannot always be approximated from the equatorial zonal-mean, time-mean atmospheric energy flux (Bischoff & Schneider, 2016). In other words, C1.13 illustrates that a double ITCZ is not always associated with an equatorward AET by the mean circulation. Previous studies have also highlighted the contribution of total AET from transient eddies. Byrne and Schneider (2016b) concluded that atmospheric eddies affect ITCZ width, while Xiang et al. (2018) showed a strong atmospheric transient eddy response when imposing shortwave radiative forcing across the Southern Ocean or southern tropics. It should also be noted that the balance between the diagnosed AEI and total AET does not hold locally in the MetUM

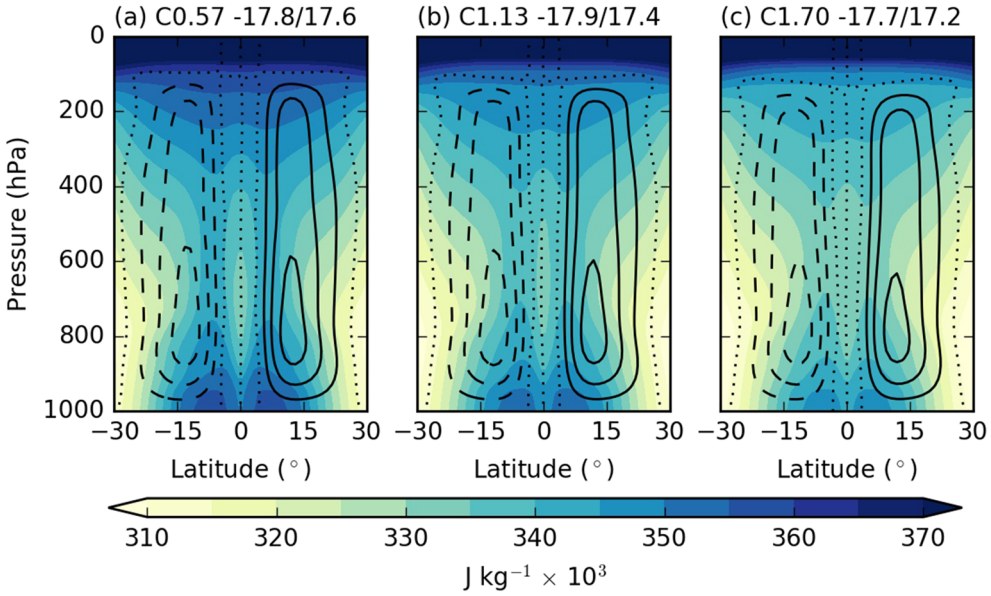

Figure 4. Zonal-mean, time-mean mass meridional stream function (kg s^{-1}) (line contours), and moist static energy (J kg^{-1}) (filled contours) for (a) C0.57, (b) C1.13, and (c) C1.70. Line contours are in intervals of 5 ×10^{10}, with dashed and dotted contours representing negative and zero values, respectively. Positive stream function values indicate clockwise circulation. Maximum magnitude of the mass meridional stream function in the SH and NH (×10^{10}) is shown in the title of each panel.

(Figure 5a). Possible reasons for this were discussed in Talib et al. (2018); the local imbalance does not affect conclusions in this study.

3.2. Sensitivity of ITCZ to Convective Mixing

This section discusses the sensitivity of the ITCZ to f_{dp} in interactive-OET simulations (Table 1). As in C1.13, C0.57 and C1.70 produce a double ITCZ (Figures 3a and 4) associated with negative AEI_0 (Figure 3b). Decreasing f_{dp} intensifies the ITCZ, defined as the maximum tropical precipitation rate, expands the ITCZ poleward, and warms tropical SSTs (Figures 3a and 3c).

The sensitivity of tropical SSTs to f_{dp} is investigated by partitioning the globally integrated net-downward surface energy flux into clear-sky and cloudy-sky radiative fluxes and surface turbulent fluxes throughout the entire simulation, including the accelerated coupling period (Figure 6a). Initially, a greater net-downward surface energy flux of 5 W m^{-2} is simulated in C0.57 compared to C1.70 due to differences in cloudy-sky radiation (Figure 6a). Below approximately 500 hPa, decreasing f_{dp} increases downward SW cloudy-sky radiation (filled contours in Figure 6b) associated with decreased cloud-ice and cloud-liquid concentrations in convective regions (filled and lined contours, respectively, in Figure 6c). Decreased f_{dp} is associated with increased plume buoyancy and less lower- and middle-tropospheric moisture detrainment from convective plumes. At lower f_{dp}, more convective plumes reach the tropopause, where forced detrainment moistens the upper troposphere. This increase in downward SW cloudy-sky radiation is greater than the decrease associated with increased upper-tropospheric (approximately 150 hPa) cloud fraction and cloud ice (Figures 6b and 6c). Other components of the net-downward surface energy flux respond on longer timescales and eventually counteract the initial decrease in net-downward surface energy flux (Figure 6a). The steady-state ocean heat content is achieved when changes in other surface energy flux components balance the cloudy-sky radiation changes. The increase in mean tropical SST when decreasing f_{dp} increases total MSE across the tropics (Figure 4). The mean circulation is more efficient at transporting MSE at lower f_{dp} due to a deeper mean circulation rather than an increased MSE difference between the boundary layer and upper troposphere (not shown).

Similar to the argument proposed for atmosphere-only simulations (Talib et al., 2018), reducing f_{dp} decreases the minimum boundary layer MSE needed for deep convection, encouraging convection over cooler SSTs

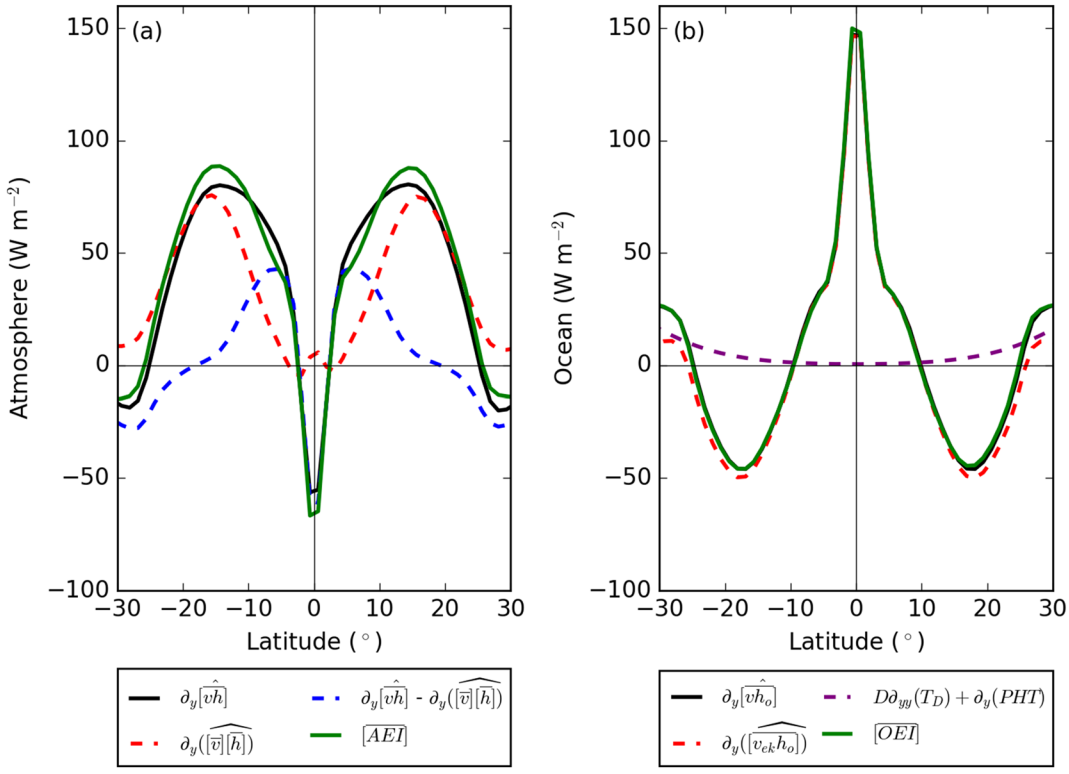

Figure 5. (a) Components of meridional divergence of atmospheric MSE flux and AEI (W m^{-2}) in C1.13. The solid black line denotes meridional divergence of total MSE flux ($\partial_y[\widehat{\overline{vh}}]$); the red dashed line denotes meridional divergence of MSE flux due to mean circulation ($\partial_y(\widehat{[\overline{v}][\overline{h}]})$); the blue dashed line denotes meridional divergence of MSE flux due to eddies ($\partial_y[\widehat{\overline{vh}}] - \partial_y(\widehat{[\overline{v}][\overline{h}]})$); and the solid green line denotes zonal-mean, time-mean AEI. [], $\bar{}$ and $\hat{}$ denote the zonally averaged, time-averaged, and vertically integrated value, respectively. (b) Components of meridional divergence of ocean energy flux (W m^{-2}) and OEI (W m^{-2}) in C1.13. The solid black line denotes meridional divergence of total energy flux and includes extratropical prescribed q flux and diffusion ($\partial_y[\widehat{\overline{vh_o}}]$); the red dashed line denotes meridional divergence of ocean energy flux due to the mean Ekman-driven circulation ($\partial_y(\widehat{[\overline{v_{ek}}][\overline{h_o}]})$); the violet dashed line denotes meridional divergence of ocean energy flux due to diffusion and extratropical prescribed q flux; and the solid green line denotes zonal-mean, time-mean OEI. h_o denotes the energy at each ocean grid point (C_pT).

and broadening the ITCZ. This argument for why the ITCZ broadens when decreasing f_{dp} does not explain the sensitivity of the ITCZ intensity (Figure 3a). Greater tropical precipitation rates at lower f_{dp} are due to warmer tropical SSTs (Figure 3c) associated with increased surface latent heat fluxes (Figure 7d) and atmospheric moisture (not shown); there are minimal changes in moisture export out of the tropics (not shown). Decreasing f_{dp} also increases the meridional SST gradient across the equatorial region (Figure 3c), associated with a broader region of minimal precipitation (Figure 3a) and increased equatorward eddy-associated latent energy transport at low latitudes (not shown).

AEI_0 is highly insensitive to f_{dp} in interactive-OET simulations (Figure 3b), indicative of a minimal sensitivity of low-latitude AET. To understand this, budgets for the net-downward TOA flux, AEI and OEI are calculated (Figure 7). For OEI the sign is reversed (Figures 7g–7i) so that all energy fluxes are positive into the atmosphere. As in atmosphere-only prescribed-SST simulations (Talib et al., 2018), latent heat fluxes and cloudy-sky radiative fluxes are most sensitive to f_{dp} (Figures 7d and 7f). Decreasing f_{dp} from 1.13 to 0.57 decreases equatorial cloudy-sky AEI_0 (Figure 7d) associated with the preference for off-equatorial convection (Figure 3a). This decrease is offset by increased latent heat fluxes (Figure 7d) associated with warmer SSTs (Figure 3c). Coupled simulations reveal that interactive SSTs limit the sensitivity of AEI_0 to f_{dp}. However, even though coupling reduces the sensitivity of AEI_0 to f_{dp}, the net-downward TOA energy flux remains substantially sensitive to f_{dp} (Figures 7a and 7c). The sensitivity of the net-downward TOA

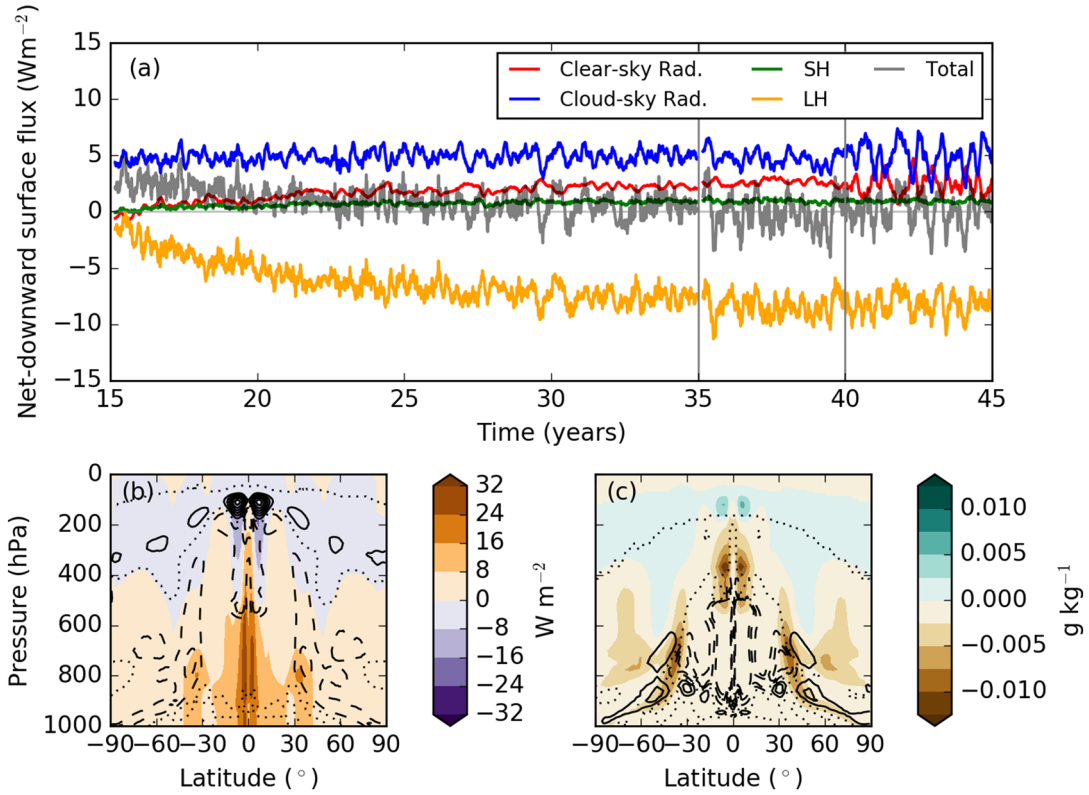

Figure 6. C0.57 minus C1.70 for (a) zonal-mean evolution of the globally averaged net-downward surface energy flux and its components (W m^{-2}). In (a) a 60-day running mean is shown. Vertical gray lines at 35 and 40 years indicate the end of the accelerated coupling and the analysis periods, respectively. The lines show changes in clear-sky radiation (red), cloudy-sky radiation (blue), surface sensible heat flux (green), surface latent heat flux (orange), and the total of all components (black). Panels (b) and (c) show zonal-mean, time-mean differences during the analysis period (final five years) in (b) cloud fraction (lines, 5% intervals), downward SW cloud radiative flux (filled, W m^{-2}); (c) cloud-liquid (lines, 0.002 g kg^{-1}) and cloud-ice concentrations (filled, g kg^{-1}). Dashed and dotted contours represent negative and zero values, respectively.

energy flux is determined by changes in AEI and OEI. In coupled simulations, OEI is more sensitive than AEI to f_{dp} across the tropics (Figures 7d, 7f, 7g, and 7i) implying that OET changes play a role in the reduced sensitivity of the ITCZ to f_{dp} when coupling.

Coupled simulations in this study highlight a smaller sensitivity of the ITCZ to convective mixing compared to atmosphere-only simulations in previous studies (Mobis & Stevens, 2012; Oueslati & Bellon, 2013; Talib et al., 2018). However, it is difficult to conclude that coupling is primarily responsible for the reduced sensitivity, as coupled simulations here have substantially different SST profiles to that prescribed in atmosphere-only simulations (Talib et al., 2018).

3.3. The Effect of Prescribing SST on the Sensitivity of the ITCZ to Convective Mixing

To explore the effect of atmosphere-ocean coupling on the sensitivity of the ITCZ to f_{dp}, nine 3-year prescribed-SST aquaplanet simulations are performed (Table 2). The 3-year length is consistent with the atmosphere-only simulations in Talib et al. (2018). The first 2 months of each simulation are discarded as spin-up; the remaining 2 years and 10 months are analyzed. The zonal-mean, time-mean SST profiles from the interactive-OET simulations are prescribed. These profiles are labeled "PS" (prescribed SST) followed by the f_{dp} value in the interactive-OET simulation from which the prescribed SSTs are taken (Figure 3c). For each prescribed SST profile (PS0.57, PS1.13, and PS1.70), three simulations are performed with f_{dp} varied to 0.57, 1.13, and 1.70 (Table 2), as in the interactive-OET simulations (Table 1). Prescribing SSTs from the coupled experiment with the same value of f_{dp} simulates a similar meridional structure of precipitation and AEI. For example, precipitation and AEI in F0.57PS0.57 (Figures 8a and 8b) are similar to C0.57

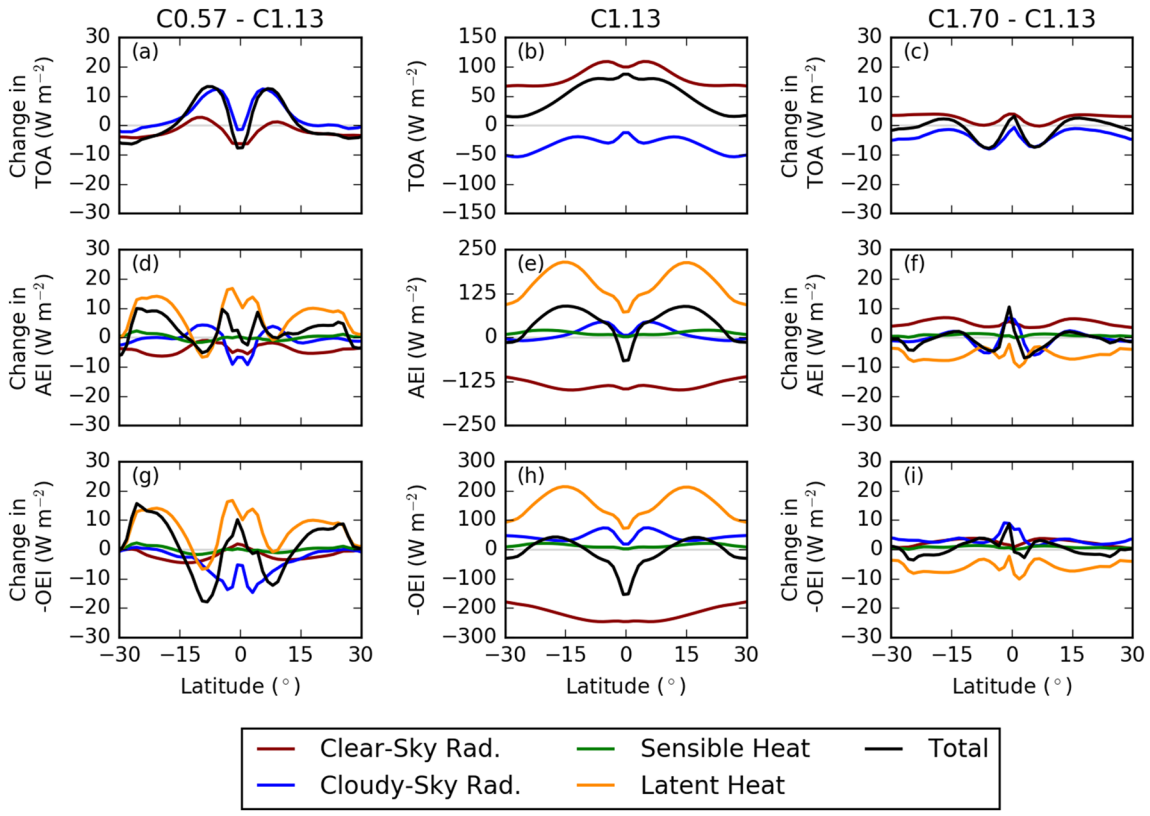

Figure 7. Zonal-mean, time-mean of components of (a–c) net-downward TOA flux (W m^{-2}), (d–f) AEI (W m^{-2}), and (g–i) −1 × OEI (W m^{-2}). Panels in the first and third columns show the changes between C0.57 and C1.13 and between C1.70 and C1.13, respectively. Panels in second column show C1.13. The lines show clear-sky radiation (red), cloudy-sky radiation (blue), surface sensible heat flux (green), surface latent heat flux (orange), and the total of all components (black).

(Figures 3a and 3b). Similarities between coupled and prescribed-SST simulations indicate that mean SSTs are important in determining atmospheric conditions; transient SST variability plays a minimal role.

All nine prescribed-SST simulations produce a double ITCZ with negligible equatorial precipitation (Figures 8a, 8c, and 8e), negative AEI_0 (Figures 8b, 8d, and 8f), and equatorial subsidence (not shown). The ITCZ broadens as f_{dp} decreases regardless of SST (Figures 8a, 8c, 8e, and 9c). Tropical free-tropospheric MSE is insensitive to f_{dp} (not shown), hence reducing f_{dp} decreases the boundary layer MSE required for deep convection, strengthening convection over cooler SSTs and expanding the ITCZ poleward. Similar behavior is seen for the Qobs SST profile (Talib et al., 2018).

Comparing interactive-OET and PS1.13 simulations reveals that coupling decreases the sensitivity of the ITCZ location and width to f_{dp} (Figures 9 and 10a). For example, the poleward ITCZ shift is greater by 1.7° latitude between F1.70PS1.13 and F0.57PS1.13 compared to C1.70 and C0.57 (Figure 9d). The reduced sensitivity of the ITCZ location when coupling is associated with a sensitivity of meridional SSTs to f_{dp}. Decreasing f_{dp} in interactive-OET simulations increases the meridional SST gradient between the tropical SST maximum and approximately 15° latitude (Figure 3c). This promotes convection further equatorward. Assuming a minimal circulation sensitivity to f_{dp} and that the SST profile determines boundary layer MSE, an increased SST gradient increases the gradient of boundary layer MSE, which restricts deep convection to a smaller range of latitudes close to the equatorial maximum in MSE where the minimum boundary layer MSE required for deep convection can be surpassed. The reduced boundary layer MSE required for deep convection at lower f_{dp} (Mobis & Stevens, 2012; Talib et al., 2018), which promotes

Table 2
Prescribed-SST Simulations Using Simulated Zonal-Mean, Time-Mean SSTs From Interactive-OET Simulations (Table 1)

		Prescribed SSTs		
		PS0.57	PS1.13	PS1.70
f_{dp}	0.57	F0.57PS0.57	F0.57PS1.13	F0.57PS1.70
	1.13	F1.13PS0.57	F1.13PS1.13	F1.13PS1.70
	1.70	F1.70PS0.57	F1.70PS1.13	F1.70PS1.70

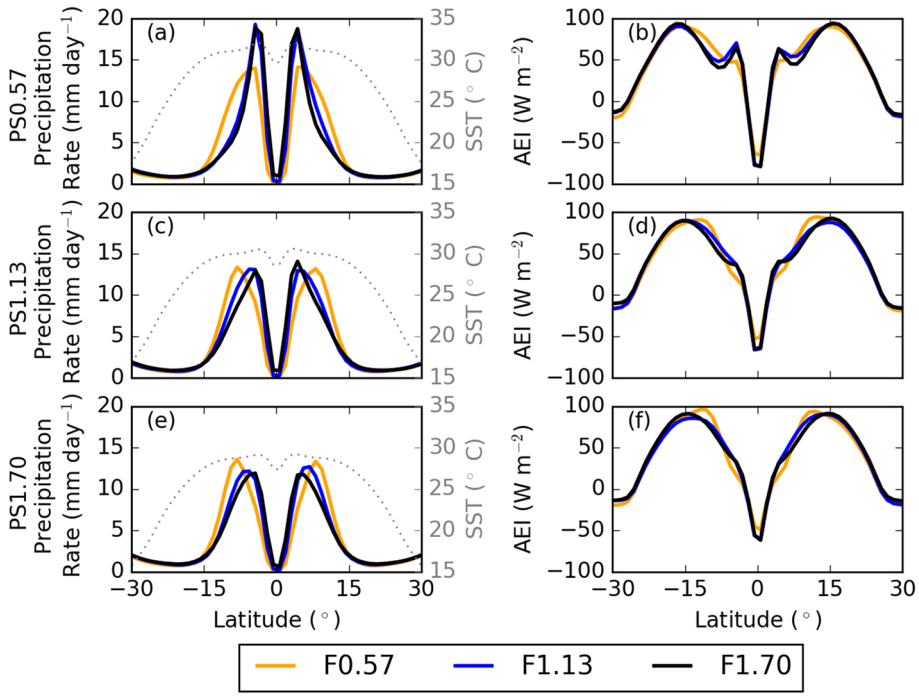

Figure 8. Zonal-mean, time-mean (a, c, and e) precipitation rates (solid lines, mm day^{-1}) and prescribed SSTs (gray dotted, °C), and (b, d, and f) AEI (W m^{-2}) in (a, b) PS0.57, (c, d) PS1.13, and (e, f) PS1.70 simulations. Orange, blue, and black lines denote f_{dp} equals 0.57, 1.13, and 1.70, respectively.

convection at higher latitudes, is offset by a stronger meridional SST gradient which restricts convection to lower latitudes. Coupling also decreases the sensitivity of AEI and AET to f_{dp} across the equatorial and ITCZ region ($\leq$10° latitude; Figures 10b and 10f), associated with a weaker response of cloudy-sky radiation and latent heat fluxes (Figures 10d and 10e). However, it should it be noted that coupling increases the sensitivity of the ITCZ intensity (Figure 9b) due to changes in mean tropical SST (section 3.2).

The sensitivity of the ITCZ location and width to f_{dp} is similar in prescribed-SST simulations regardless of SST profile: decreasing f_{dp} broadens and shifts the ITCZ poleward (Figures 8a, and 9c and 9e). However, due to the close proximity of the ITCZ to the tropical SST maximum in PS0.57 simulations, the sensitivity of the ITCZ intensity is greater in PS0.57 simulations compared to PS1.13 and PS1.70 simulations. In PS0.57 simulations, the ITCZ is collocated with the SST maximum when f_{dp} equals 1.13 and 1.70. As the ITCZ cannot contract equatorward at higher f_{dp} due to equatorial subsidence, the ITCZ intensifies by approximately 5 mm day^{-1}. The same ITCZ intensification in PS0.57 at higher f_{dp} is seen on the equator when using Qobs (Talib et al., 2018). In agreement with previous work (Bellon & Sobel, 2010; Hess et al., 1993; Mobis & Stevens, 2012), we hypothesize that the ITCZ is simulated closer to the equator in PS0.57 than PS1.13 and PS1.70 due to a larger meridional SST gradient across the deep tropics ($\pm$10° latitude) in PS0.57 (not shown). When using PS0.57, the minimum boundary layer MSE required for deep convection is achieved closer to the equator, resulting in a more equatorward ITCZ.

Our prescribed-SST simulations illustrate two reasons why the AEI framework (Bischoff & Schneider, 2016) should be used with caution to understand the tropical atmosphere. First, for some SST profiles increased, less negative AEI_0 is not associated with an equatorward contraction of the double ITCZ (Figure 8). For example, decreasing f_{dp} under PS0.57 increases AEI_0 but shifts the ITCZ poleward. Increased AEI_0 is driven by increased latent heat fluxes (Figure 11) and a drier equatorial lower atmosphere. Second, as in interactive-OET simulations (section 3.1), equatorward AET at low latitudes is predominantly achieved by eddies (not shown). Hence, it appears that the increased role of eddies in prescribed-SST and interactive-OET simulations is associated with the equatorial SST minimum and double ITCZ (Figures 8a, 8c, and 8e), as well as a local equatorial minimum in specific humidity (not shown). Changes in MSE flux with f_{dp} are also predominantly associated with eddies (not shown).

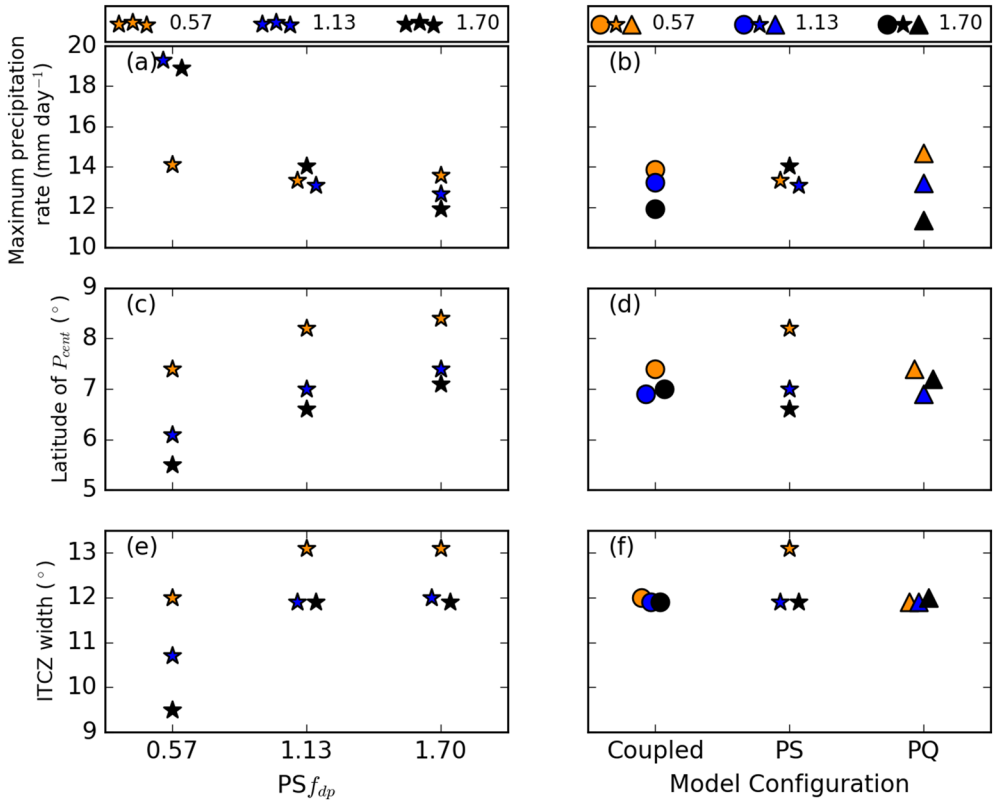

Figure 9. Zonal-mean, time-mean (a, b) maximum precipitation rate (mm day^{-1}), (c, d) latitude of P_{cent}, and (e, f) ITCZ width (°) in (a, c, and e) prescribed-SST simulations and (b, d, and e) when comparing different model configurations. P_{cent} is the median of zonal-mean precipitation between 0° and 20°N (Hwang & Frierson, 2010) while the ITCZ width is the meridional distance between the ascending branch of the Hadley circulation and the local maximum in mass meridional stream function (Byrne & Schneider, 2016a). Both diagnostics are interpolated to a 0.1° grid. Circles, stars and triangles denote interactive-OET, prescribed-SST and prescribed-OET simulations, respectively. Orange, blue and black symbols denote simulations where f_{dp} equals 0.57, 1.13 and 1.70, respectively. In (a), (c), and (e) the x axis corresponds to the f_{dp} value used in the coupled simulation in which the prescribed SSTs are taken from, while in (b), (d), and (f) the x axis corresponds to the modeling configuration. In (b), (d), and (f) PS1.13 simulations are chosen to compare different model configurations.

3.4. Sensitivity of the ITCZ to Convective Mixing With a Prescribed Ocean Energy Transport

Interactive OET reduces the sensitivity of the ITCZ to hemispherically asymmetric forcing (Green & Marshall, 2017; Hawcroft et al., 2017; Tomas et al., 2016). To explore the effect of interactive OET on the sensitivity of the ITCZ to convective mixing, coupled simulations with a prescribed Ekman-driven q-flux are performed ("prescribed-OET simulations," Table 3.4). Prescribing OET disables the dynamic ocean response while retaining thermodynamic atmosphere-ocean interactions. The prescribed Ekman-driven q-flux is added to the extratropical q flux (section 2.1). OET is prescribed in the ocean mixed layer at all latitudes using the zonal-mean, time-mean temperature tendencies from the Ekman-driven circulation in an interactive-OET simulation. Temperature tendencies from vertical mixing are also prescribed, decoupling the two ocean layers and reducing the time to achieve equilibrium. Three prescribed-OET (PQ) simulations are initialized from the end of C1.13 with the prescribed Ekman-driven q-flux from C1.13, with f_{dp} set to the values used in interactive-OET simulations: C0.57PQ1.13, C1.13PQ1.13, and C1.70PQ1.13 (Table 1). Ten years of accelerated coupling are followed by 10 years of normal simulation, the final 5 years of which are analysed. C1.13 and C1.13PQ1.13 have a similar mean state (comparing blue lines in Figures 3 and 12), demonstrating that prescribing the time-mean Ekman-driven q flux does not substantially change the mean tropical atmosphere. As OEI is sensitive to f_{dp} (section 3.2), it is hypothesized that prescribing the Ekman-driven q flux will make AEI and the ITCZ more sensitive to f_{dp} due to constrained OET and OEI.

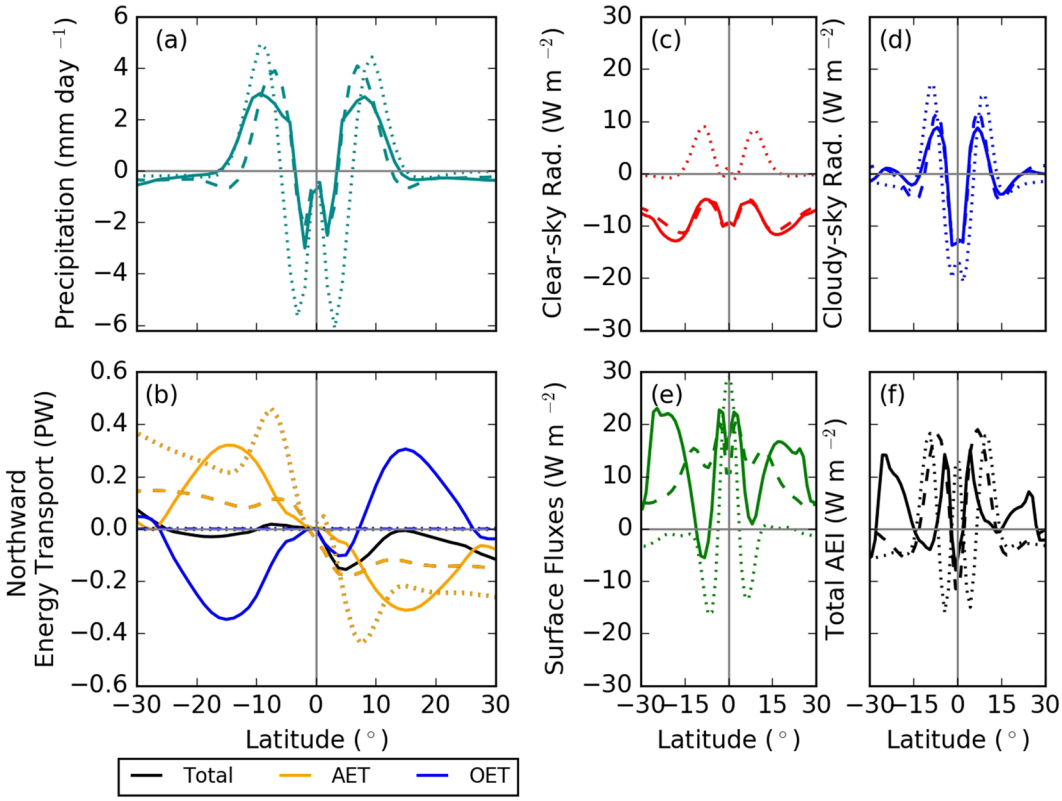

Figure 10. Differences in (a) precipitation (mm day^{-1}), (b) total (black), atmospheric (yellow), and oceanic (blue) energy transports (PW), (c) clear-sky radiation AEI, (d) cloudy-sky radiation AEI, (e) surface fluxes AEI (including surface and latent heat fluxes) and (f) total AEI, when decreasing f_{dp} from 1.70 to 0.57. Solid lines denote interactive-OET simulations, dotted lines denote prescribed-SST simulations (PS1.13), and dashed lines denote prescribed-OET simulations. In (b) total energy transport change is only shown for coupled simulations. In (e) surface flux changes are predominantly associated with latent heat fluxes.

As in interactive-OET and prescribed-SST simulations, all three prescribed-OET simulations produce a double ITCZ (Figure 12a), negative AEI_0 (Figure 12b), equatorial subsidence (not shown), and an equatorward AET at low latitudes. The prescribed Ekman-driven q flux produces an equatorial SST minimum (Figure 12c) associated with a equatorial minimum in boundary layer MSE and convection. As in interactive-OET simulations (section 3.2) latent energy transport associated with transient eddies dominates equatorward AET at low latitudes, not the mean circulation (not shown)

Prescribing the Ekman-driven OET constrains OEI at equilibrium (Figure 13). In both interactive and prescribed-OET simulations, decreasing f_{dp} reduces the reflection of SW radiation by clouds (Figure 6) and increases surface absorption of cloudy-sky radiation (Figure 13g). In interactive-OET simulations, OET changes can partly compensate for changes in net-downward surface radiation. However, in prescribed-OET simulations, other components of the net-downward surface energy flux must respond to these cloudy-sky radiation changes. Latent heat fluxes play the dominant role and increase across the tropics (Figures 13g and 10e). Comparing the sensitivity of energy budgets to f_{dp} between interactive-OET and prescribed-OET simulations (Figures 7 and 13) reveals that prescribing OET increases the sensitivity of AEI to f_{dp} equatorward of 10° (Figure 10f). For example, prescribed-OET simulations show a stronger decrease in AEI_0 by 5 W m^{-2} when decreasing f_{dp} from 1.70 to 0.57 (Figure 10f). However, the sensitivity of the ITCZ structure and components of AEI are much greater when prescribing SST compared to prescribing OET highlighting the importance of interactive atmosphere-ocean interactions.

Prescribing OET increases the sensitivity of AEI to f_{dp} (Figure 10f), suggesting that prescribing OET increases the sensitivity of the ITCZ to f_{dp}. However, the change in sensitivity depends on the chosen metric (Figure 9). Prescribing OET does not affect the sensitivity of the ITCZ location and width (Figures 9d and 9f).

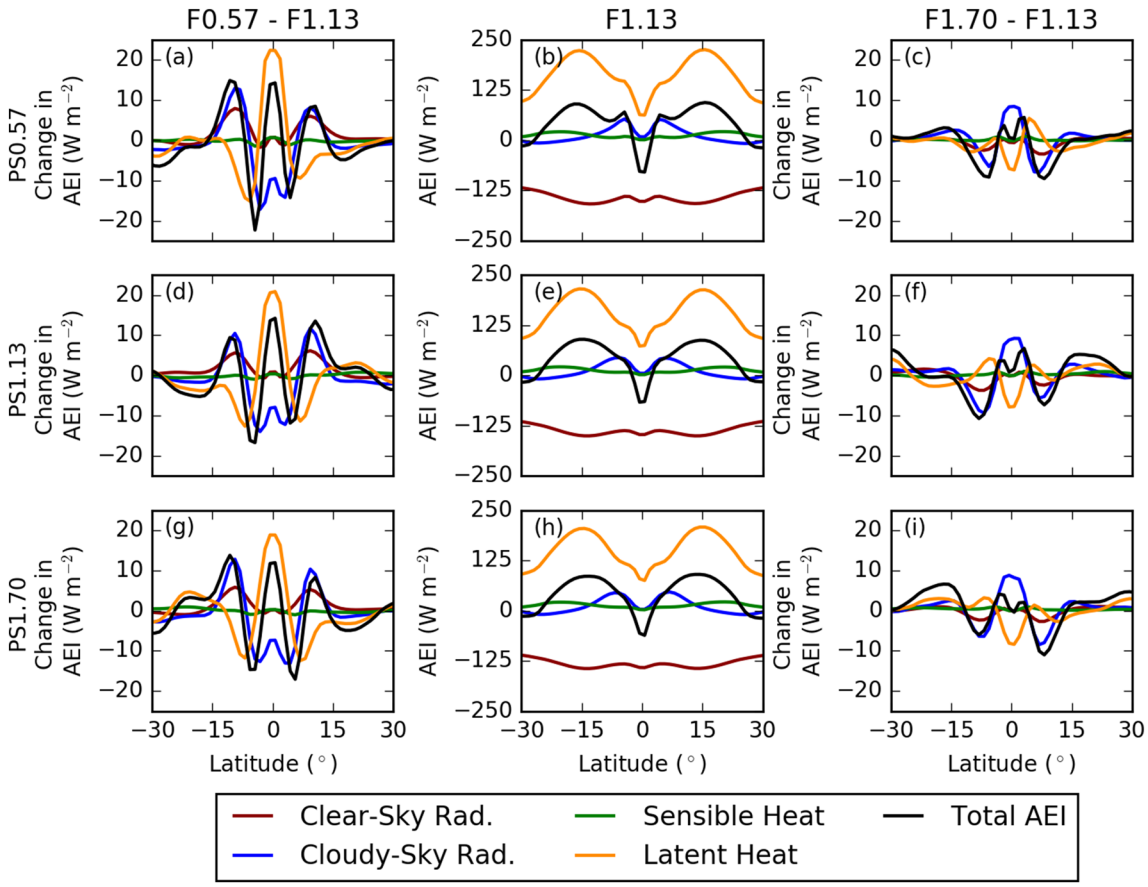

Figure 11. Zonal-mean, time-mean AEI (W m^{-2}) budgets in (a–c) PS0.57, (d–f) PS1.13, and (g–i) PS1.70 simulations. Panels in the first and third columns show the changes between *F*0.57 and *F*1.13 and between *F*1.70 and *F*1.13, respectively. Panels in second column show *F*1.13 simulations. The lines show clear-sky radiation (red), cloudy-sky radiation (blue), surface sensible heat flux (green), surface latent heat flux (orange), and the total of all components (black).

Decreasing f_{dp} may decrease AEI_0 more in prescribed-OET simulations, which requires a more equatorward AET, but increased AET is predominantly achieved by eddies. Therefore, the ITCZ location does not change. However, prescribing OET does increase the sensitivity of ITCZ intensity to f_{dp} (Figure 9b). Greater increases in tropical latent heat flux occurs in prescribed-OET simulations than in interactive-OET simulations when decreasing f_{dp} (Figure 10e), as increased surface absorption of cloudy-sky radiation (Figure 13g) cannot be offset by OET changes. Increased tropical latent heat fluxes are associated with an intensified ITCZ (Figure 12). Prescribed-OET simulations reveal that feedbacks via changes in OET affect the sensitivity of the ITCZ to a change in an atmospheric process or feedback. As a result, we advise against using prescribed-OET simulations to understand the sensitivity of the ITCZ to an atmospheric process or feedback.

4. Discussion

MetUM GA6.0 coupled to an idealized two-layer ocean model with an interactive Ekman-driven OET simulates a double ITCZ for all convective mixing rates used. Ekman-driven oceanic upwelling reduces equatorial SSTs and boundary layer MSE, promoting a double ITCZ (Codron, 2012; Pike, 1971). We hypothesize that a double ITCZ and negative AEI_0 would be simulated at any convective mixing rate in our coupled model configuration, due to small upward equatorial surface heat fluxes associated with an equatorial SST minimum. Coupling reduces the sensitivity of the ITCZ location and width to convective mixing, as has been shown for other atmospheric processes and forcings (Green & Marshall, 2017; Oueslati & Bellon, 2013; Tomas et al., 2016).

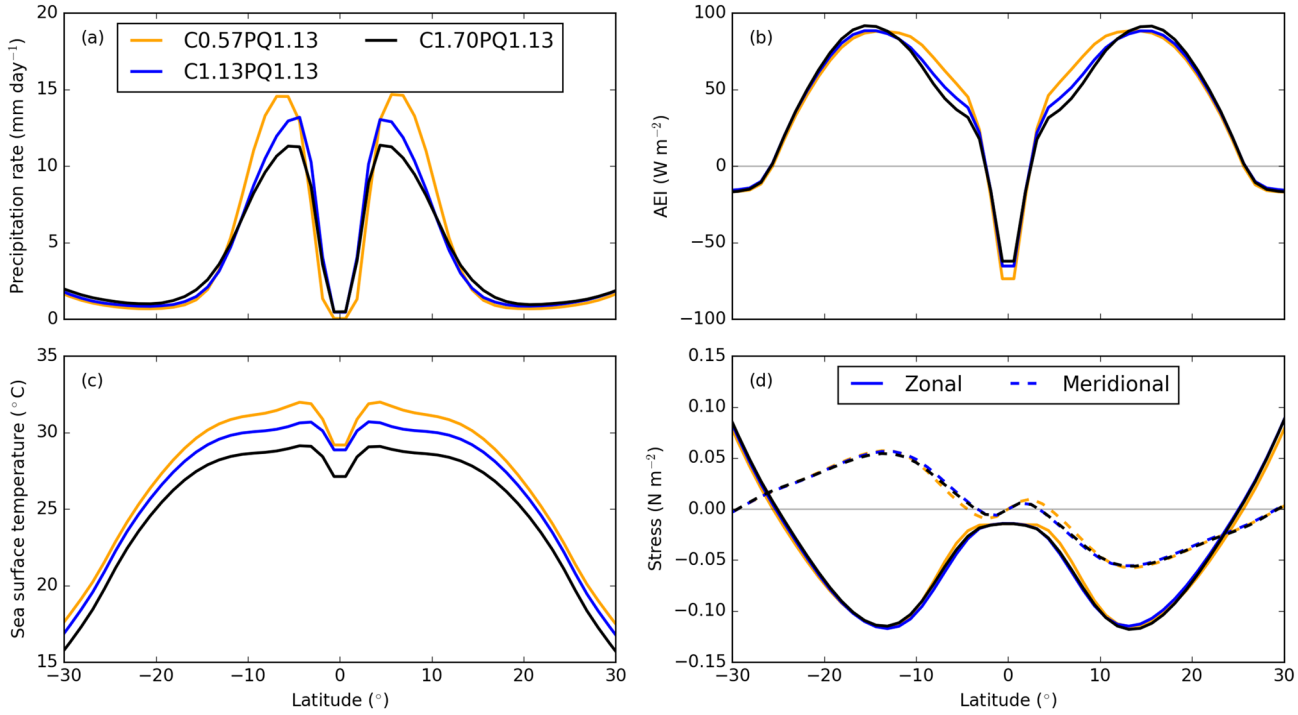

Figure 12. Zonal-mean, time-mean tropical (a) precipitation (mm day^{-1}), (b) AEI (W m^{-2}), (c) SSTs (°C), and (d) zonal (solid) and meridional (dashed) wind stresses (N m^{-2}) in prescribed-OET simulations (Table 3).

While previous studies argue that OET changes reduce the sensitivity of the ITCZ to hemispherically asymmetric forcing (Green & Marshall, 2017; Hawcroft et al., 2017; Kang et al., 2018; Kay et al., 2016; Tomas et al., 2016), here the reduced sensitivity of the ITCZ to f_{dp} when coupling is due to interactive SSTs. Decreasing convective mixing increases the tropical-mean SST and near-equatorial meridional SST gradient, while the sensitivity of OET to convective mixing is too small to substantially affect the sensitivity of the ITCZ to convective mixing. In agreement with Mobis and Stevens (2012), increasing the meridional SST gradient promotes convection at lower latitudes. Prescribed-SST simulations in Talib et al. (2018) show that decreasing mixing is associated with an ITCZ expansion due to a reduced minimum boundary layer MSE required for deep convection. However, in coupled simulations, this effect is offset by the effect of meridional SST gradient changes. The reduced sensitivity of the ITCZ to convective mixing with coupling in Oueslati and Bellon (2013), who used a full configuration of CNRM-CM5, is consistent with this study. The effect of atmosphere-ocean coupling in Oueslati and Bellon (2013) may also be partly due to SST changes. While atmosphere-ocean coupling reduces the sensitivity of the ITCZ location to convective mixing, the ITCZ stills widens as mixing decreases. This is consistent with Hirota et al. (2011) who argue that CMIP3 models with weak convective mixing have a double ITCZ bias with too much precipitation in subsidence regions. Our coupled simulations reveal that sensitivities of the ITCZ to an atmospheric forcing or process derived from atmosphere-only simulations do not necessarily apply to coupled simulations and the real world.

As SST changes decrease the sensitivity of the ITCZ location and width when coupling, prescribing OET does not affect the sensitivity of the ITCZ location. However, prescribing OET constrains the total OEI at equilibrium. As a result, stronger latent heat fluxes at lower mixing rates are associated with an intensified ITCZ. Hence, prescribing OET increases the sensitivity of the ITCZ intensity to convective mixing. The difference between prescribed and interactive-OET simulations highlights that prescribed-OET simulations should be avoided to understand the sensitivity of the real-world ITCZ to modified atmospheric forcings or processes.

Table 3
Prescribed-OET Coupled Simulations

Simulation	f_{dp}	Ekman-driven q flux
C0.57PQ1.13	0.57	Prescribed PQ1.13
C1.13PQ1.13	1.13	Prescribed PQ1.13
C1.70PQ1.13	1.70	Prescribed PQ1.13

The AEI framework (Bischoff & Schneider, 2014, 2016; Kang et al., 2008) breaks down when applied to simulations in this study. It cannot explain

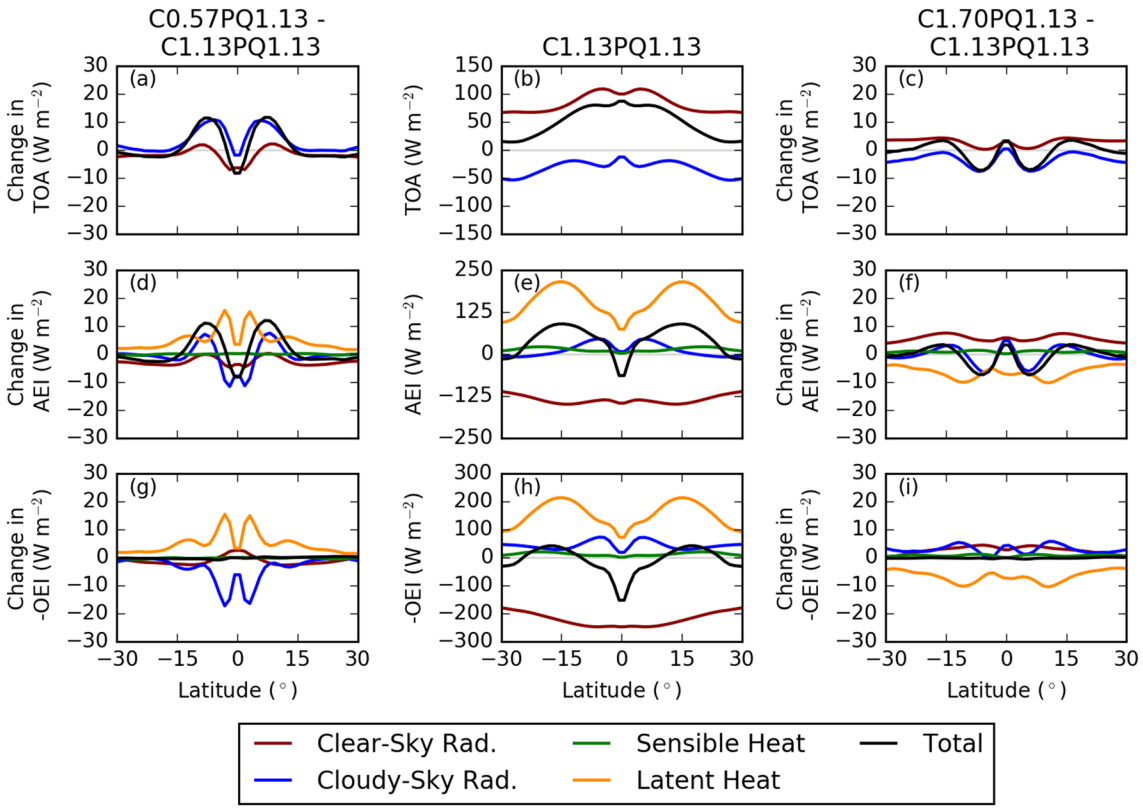

Figure 13. Zonal-mean, time-mean components of (a–c) net-downward TOA flux (W m^{-2}) (d–f) AEI (W m^{-2}), (g–i) −OEI (W m^{-2}). Panels in the first and third columns show the changes between C0.57PQ1.13 and C1.13PQ1.13 and between C1.70PQ1.13 and C1.13PQ1.13, respectively. Panels in second column show simulated values in C1.13PQ1.13. The lines show clear-sky radiation (red), cloudy-sky radiation (blue), surface sensible heat flux (green), surface latent heat flux (orange), and the total of all components (black).

the sensitivity of the ITCZ to convective mixing in interactive-OET simulations, nor the reduced sensitivity when coupling. While all experiments show a double ITCZ and negative equatorial AEI, in agreement with Bischoff and Schneider (2016), equatorward AET is achieved by transient eddies transporting latent energy, not by the mean circulation. As the mean circulation plays a minimal role in equatorward AET, the AEI framework is not useful to diagnose the ITCZ location. Table 4 presents the equatorial AEI, the location of the precipitation centroid (P_{cent}) (Frierson & Hwang, 2012), and the two energy flux equators (δ) (Bischoff & Schneider, 2016) in coupled, PS1.13, and PQ1.13 simulations. δ is the latitude of zero meridional MSE flux equals zero using a second-order Taylor expansion of the equatorial meridional MSE flux (Bischoff & Schneider, 2016). In PS1.13 simulations, decreasing mixing increases AEI_0, typically associated with an equatorward contraction of the double ITCZ (Bischoff & Schneider, 2016). However, the ITCZ expands poleward with negligible changes in the diagnosed energy flux equator (Table 4) due to changes in transient eddies being primarily responsible for changes in AET. The important contribution of atmospheric transient eddies to total AET and to the ITCZ structure is consistent with previous studies (Byrne & Schneider, 2016b; Xiang et al., 2018). Future work to understand the double ITCZ bias in GCMs and real-world ITCZ characteristics must consider the AET by eddies. The AEI framework needs to be redefined to include the contribution of AET by transient eddies.

Table 4

$[\overline{AEI}]_0$ (W m^{-2}), Location of P_{cent} (°), and Approximate Energy Flux Equator (δ, °) in Coupled, PS1.13 and PQ1.13 Simulations

Simulation	$[\overline{AEI}]_0$ (W m^{-2})	P_{cent} (°)	Energy flux equator (δ) location (°)
C0.57	−65.2	7.4	4.2/−4.2
C1.13	−65.7	6.9	4.3/−4.2
C1.70	−59.4	7.0	4.2/−4.4
F0.57PS1.13	−51.7	8.2	4.4/−4.1
F1.13PS1.13	−65.6	7.0	4.3/−4.3
F1.70PS1.13	−64.4	6.6	4.3/−4.0
C0.57PQ1.13	−73.6	7.4	4.3/−4.3
C1.13PQ1.13	−65.3	6.9	4.2/−4.3
C1.70PQ1.13	−62.1	7.2	4.3/−4.3

Note. P_{cent} is the median of zonal-mean precipitation between 0° and 20° N (Hwang & Frierson, 2010), while δ is computed using the zonal-mean, time-mean cross-equatorial atmospheric energy flux and equatorial AEI following Bischoff and Schneider (2016).

Our conclusions may depend on the design of the two-layer ocean model. Prescribed-SST simulations reveal that the sensitivity of the ITCZ to

convective mixing depends on SSTs. Hence, changes in model design that affect SST may change the sensitivity of the ITCZ to convective mixing, including: changes in the prescribed OET profile; introducing zonal asymmetries in SST and surface fluxes; inserting landmasses; adding seasonally varying insolation; and changing the specification of the near-equatorial Coriolis parameter in the calculation of the Ekman velocity. Oueslati and Bellon (2013) show that the sensitivity of the ITCZ to convective mixing in CNRM-CM5 varies zonally. Previous aquaplanet studies have also shown that introducing zonal SST asymmetries varies the ITCZ zonal structure and intensity (Nakajima et al., 2013; Neale & Hoskins, 2001b). Following these studies, we hypothesize that zonal SST asymmetries will change the sensitivity of the ITCZ to convective mixing. For example, when the ITCZ is collocated with the SST maximum, increasing f_{dp} will intensify the ITCZ. However, if the ITCZ is poleward of the SST maximum, increasing f_{dp} will shift the ITCZ closer to the warmest SSTs. In the real world, zonal asymmetries in tropical SSTs affect the ITCZ and the influence of Ekman-driven upwelling on SSTs. For example, over the Pacific Ocean easterly trade winds develop SST gradients between the West and East Pacific (Bjerknes, 1969). Zonal tropical SST variations change the tropical rainfall structure (Dai, 2006), the influence of Ekman-driven upwelling, and the sensitivity of tropical rainfall to atmospheric forcing and parameterization changes (Hawcroft et al., 2017; Oueslati & Bellon, 2013; Tomas et al., 2016). GCM experiments in this study have also disregarded zonal and meridional surface temperature asymmetries associated with land. Real-world or idealized continental land and topography will lead to asymmetries in surface properties and affect both the mean state and zonal variations of ITCZ characteristics. Codron (2012) performed GCM experiments with idealized continental land, using an atmospheric model coupled to a two-layer ocean model that resolves the Ekman-driven OET. Introducing land led to zonal variations in ITCZ characteristics, including a dry equatorial belt across the Pacific Ocean and increased precipitation on the western edge of continental land.

Understanding what controls ITCZ characteristics remains a fundamental question in climate science (Bony et al., 2015) and has motivated several model intercomparison projects including prescribed-SST aquaplanet simulations in CMIP5 (Coupled Model Intercomparison Project Phase 5; Voigt & Shaw, 2015) and aquaplanet slab ocean simulations with a prescribed q flux in TRACMIP (Tropical Rain belts with an Annual cycle and a Continent; Voigt et al., 2016). Alongside these studies, ETIN-MIP (Extratropical-Tropical Interaction Model Intercomparison Project) uses state-of-the-art coupled climate models to investigate model variability in the sensitivity of the ITCZ to variations in shortwave radiation forcing (Kang et al., 2019). As interactive OET reduces the sensitivity of the ITCZ to an atmospheric forcing or parameterization (Green & Marshall, 2017; Tomas et al., 2016), an idealized model intercomparison project with an interactive OET is planned (Kucharski et al., 2018), to investigate if an interactive OET changes the intermodel variability of the tropical circulation. Here, an interactive OET substantially reduces the sensitivity of the ITCZ location to convective mixing. As variations in the representation of convection plays a key role in the intermodel variability of tropical precipitation, we hypothesize that including an interactive OET will reduce intermodel variability. However, the effect of an interactive OET will depend on the ocean model design; here, the model design favors a double ITCZ. If a single ITCZ were favored due to a weaker equatorial SST minimum, then the ITCZ structure and location may have been more sensitive to convective mixing. Further idealized experiments are required before commencing a model intercomparison project in an aquaplanet configuration with an interactive OET.

5. Conclusions

Previous studies have shown a substantial sensitivity of the ITCZ to convective mixing in simulations with prescribed SSTs. However, not only are prescribed SSTs energetically inconsistent, but several studies reveal that coupling the atmosphere to an ocean model with an interactive ocean energy transport reduces the sensitivity of the ITCZ to hemispherically asymmetric forcing. We developed an idealized coupled modeling framework to quantify the effect of coupling on the sensitivity of the ITCZ to convective mixing.

Coupling the atmosphere to an ocean model that resolves the Ekman-driven ocean energy transport promotes a double ITCZ. Ekman-driven equatorial upwelling leads to an equatorial SST minimum and reduces equatorial convection and boundary layer MSE. Previous studies have shown that a double ITCZ and negative equatorial atmospheric energy input are associated with equatorward energy transport at low latitudes by the mean circulation. However in our coupled simulations this transport is minimal; equatorward

atmospheric energy transport is accomplished by transient eddies transporting latent energy. The substantial role of eddies is associated with the near-equatorial meridional gradient in SSTs and specific humidity. The mean circulation also does not affect equatorward atmospheric energy transport when changing convective mixing. As a result, the AEI framework breaks down.

Atmosphere-ocean coupling reduces the sensitivity of the ITCZ location to convective mixing. The reduced sensitivity is predominantly associated with meridional SST profile changes; the sensitivity of ocean energy transport to convective mixing is minimal. Decreased mixing increases the meridional SST gradient in the deep tropics (10°N to 10°S latitude), which reduces off-equatorial boundary layer MSE and restricts deep convection to lower latitudes. This restriction of deep convection to near-equatorial latitudes opposes the promotion of off-equatorial convection seen in prescribed-SST simulations, which is associated with a reduced minimum boundary layer MSE required for deep convection. The reduced ITCZ response to convective mixing in coupled simulations reveals the importance of SST feedbacks for ITCZ characteristics. However, even though the sensitivity of the ocean energy transport to convective mixing is not responsible for the sensitivity of the ITCZ location to mixing in coupled simulations in this study, prescribing the ocean energy transport increases the sensitivity of the ITCZ intensity to convective mixing. Sensitivities of the ITCZ to an atmospheric process or forcing derived from prescribed-SST experiments may not apply to atmosphere-ocean coupled simulations or the real world.

Data Availability Statement

Data used in this publication are available at https://doi.org/10.6084/m9.figshare.12879671 website.

Acknowledgments

J. T. was funded by the Natural Environment Research Council (NERC) via the SCENARIO Doctoral Training Partnership (NE/L002566/1) at the University of Reading. S. J. was supported by the National Centre for Atmospheric Science, a NERC collaborative center under contract R8/H12/83/001. N. P. K. was supported by an Independent Research Fellowship from the NERC (NE/L010976/1). This work is a component of the PhD thesis by J. T. We would like to thank Rowan Sutton and Mat Collins for their comments on this work.

References

Adam, O., Bischoff, T., & Schneider, T. (2016). Seasonal and interannual variations of the energy flux equator and ITCZ. Part I: Zonally averaged ITCZ position. *Journal of Climate*, *29*(9), 3219–3230.

Bacmeister, J. T., Suarez, M. J., & Robertson, F. R. (2006). Rain reevaporation, boundary layer–convection interactions, and Pacific rainfall patterns in an AGCM. *Journal of the Atmospheric Sciences*, *63*(12), 3383–3403.

Bellon, G., & Sobel, A. H. (2010). Multiple equilibria of the Hadley circulation in an intermediate-complexity axisymmetric model. *Journal of Climate*, *23*(7), 1760–1778.

Bischoff, T., & Schneider, T. (2014). Energetic constraints on the position of the Intertropical Convergence Zone. *Journal of Climate*, *27*, 4937–4951.

Bischoff, T., & Schneider, T. (2016). The equatorial energy balance, ITCZ position, and double-ITCZ bifurcations. *Journal of Climate*, *29*(8), 2997–3013, and corrigendum, 29(19), 7167–7167.

Bjerknes, J. (1969). Atmospheric teleconnections from the equatorial Pacific. *Monthly Weather Review*, *97*(3), 163–172.

Bony, S., Stevens, B., Frierson, D. M. W., Jakob, C., Kageyama, M., Pincus, R., et al. (2015). Clouds, circulation and climate sensitivity. *Nature Geoscience*, *8*(4), 261–268.

Bush, S. J., Turner, A. G., Woolnough, S. J., Martin, G. M., & Klingaman, N. P. (2015). The effect of increased convective entrainment on Asian monsoon biases in the MetUM general circulation model. *Quarterly Journal of the Royal Meteorological Society*, *141*, 311–326.

Byrne, M. P., Pendergrass, A. G., Rapp, A. D., & Wodzicki, K. R. (2018). Response of the Intertropical Convergence Zone to climate change: Location, width, and strength. *Current Climate Change Reports*, *4*(4), 355–370.

Byrne, M. P., & Schneider, T. (2016a). Energetic constraints on the width of the Intertropical Convergence Zone. *Journal of Climate*, *29*(13), 4709–4721.

Byrne, M. P., & Schneider, T. (2016b). Narrowing of the ITCZ in a warming climate: Physical mechanisms. *Geophysical Research Letters*, *43*, 11,350–11,357. https://doi.org/10.1002/2016GL070396

Chikira, M. (2010). A cumulus parameterization with State-Dependent entrainment rate. Part II: Impact on climatology in a general circulation model. *Journal of the Atmospheric Sciences*, *67*(7), 2194–2211.

Codron, F. (2012). Ekman heat transport for slab oceans. *Climate Dynamics*, *38*(1–2), 379–389.

Dai, A. (2006). Precipitation characteristics in eighteen coupled climate models. *Journal of Climate*, *19*(18), 4605–4630.

De Szoeke, S. P., & Xie, S.-P. (2008). The tropical eastern Pacific seasonal cycle: Assessment of errors and mechanisms in IPCC AR4 coupled ocean–atmosphere general circulation models. *Journal of Climate*, *21*(11), 2573–2590.

Donohoe, A., Marshall, J., Ferreira, D., & Mcgee, D. (2013). The relationship between ITCZ location and cross-equatorial atmospheric heat transport: From the seasonal cycle to the last glacial maximum. *American Meteorological Society*, *26*, 3597–3618.

Frierson, D. M. W., & Hwang, Y. (2012). Extratropical influence on ITCZ shifts in slab ocean simulations of global warming. *Journal of Climate*, *25*, 720–733.

Green, B., & Marshall, J. (2017). Coupling of trade winds with ocean circulation damps ITCZ shifts. *Journal of Climate*, *30*(12), 4395–4411.

Hawcroft, M., Haywood, J. M., Collins, M., Jones, A., Jones, A. C., & Stephens, G. (2017). Southern Ocean albedo, inter-hemispheric energy transports and the double ITCZ: Global impacts of biases in a coupled model. *Climate Dynamics*, *48*(7), 2279–2295.

Hess, P. G., Battisti, D. S., & Rasch, P. J. (1993). Maintenance of the Intertropical Convergence Zones and the Large-Scale tropical circulation on a water-covered Earth. *Journal of the Atmospheric Sciences*, *50*(5), 691–713.

Hirota, N., Takayabu, Y. N., Watanabe, M., & Kimoto, M. (2011). Precipitation reproducibility over tropical oceans and its relationship to the double ITCZ problem in CMIP3 and MIROC5 climate models. *Journal of Climate*, *24*(18), 4859–4873.

Hwang, Y.-T., & Frierson, D. M. W. (2010). Increasing atmospheric poleward energy transport with global warming. *Geophysical Research Letters*, *37*, L24807. https://doi.org/10.1029/2010GL045440

Hwang, Y.-T., & Frierson, D. M. W. (2013). Link between the double-Intertropical Convergence Zone problem and cloud biases over the Southern Ocean. *Proceedings of the National Academy of Sciences of the United States of America*, *110*(13), 4935–4940.
Kang, S. M. (2020). Extratropical influence on the tropical rainfall distribution. *Current Climate Change Reports*, *1*, 20,172.
Kang, S. M., Hawcroft, M., Xiang, B., Hwang, Y.-T., Cazes, G., Codron, F., et al. (2019). Extratropical-Tropical interaction model intercomparison project (ETIN-MIP): Protocol and initial results. *Bulletin of the American Meteorological Society*, *100*(12), 2589–2606.
Kang, S. M., Held, I. M., Frierson, D. M. W., & Zhao, M. (2008). The response of the ITCZ to extratropical thermal forcing: Idealized slab-ocean experiments with a GCM. *Journal of Climate*, *21*(14), 3521–3532.
Kang, S. M., Shin, Y., & Xie, S.-P. (2018). Extratropical forcing and tropical rainfall distribution: energetics framework and ocean Ekman advection. *Nature Partner Journals Climate and Atmospheric Science*, *1*(1), 2–12.
Kay, J. E., Wall, C., Yettella, V., Medeiros, B., Hannay, C., Caldwell, P., & Bitz, C. (2016). Global climate impacts of fixing the southern ocean shortwave radiation bias in the community earth system model (CESM). *Journal of Climate*, *29*(12), 4617–4636.
Klingaman, N. P., & Woolnough, S. J. (2014). Using a case-study approach to improve the Madden-Julian oscillation in the Hadley Centre model. *Quarterly Journal of the Royal Meteorological Society*, *140*(685), 2491–2505.
Kucharski, F., Pirani, A., Tompkins, A., Biasutti, M., Voigt, A., Byrne, M., & Farneti, R. (2018). *WCRP grand challenge on clouds, circulation and climate sensitivity: 2nd meeting on monsoons and tropical rain belts. International Centre for Theorectical Physics*.
Levitus, S. (1987). Meridional Ekman heat fluxes for the world ocean and individual ocean basins. *Journal of Physical Oceanography*, *17*(9), 1484–1492.
Lin, J. L. (2007). The double-ITCZ problem in IPCC AR4 coupled GCMs: Ocean-atmosphere feedback analysis. *American Meteorological Society*, *20*, 4497–4525.
Merlis, T. M., Schneider, T., Bordoni, S., & Eisenman, I. (2013). Hadley circulation response to orbital precession. Part I: Aquaplanets. *Journal of Climate*, *26*(3), 740–753.
Mobis, B., & Stevens, B. (2012). Factors controlling the position of the Intertropical Convergence Zone on an aquaplanet. *Journal of Advances in Modeling Earth Systems*, *4*, M00A04. https://doi.org/10.1029/2012MS000199
Nakajima, K., Yamada, Y., Takahashi, Y. O., Ishiwatari, M., Ohfuchi, W., & Hayashi, Y.-Y. (2013). The variety of forced atmospheric structure in response to tropical SST anomaly in the aqua-planet experiments. *Journal of the Meteorological Society of Japan*, *91*, 143–193.
Neale, R., & Hoskins, B. (2001a). A standard test for AGCMs including their physical parametrizations: I: The proposal. *Atmospheric Science Letters*, *1*, 101–107.
Neale, R., & Hoskins, B. (2001b). A standard test for AGCMs including their physical parametrizations. II: Results for the Met Office model. *Atmospheric Science Letters*, *1*(2), 108–114.
Oueslati, B., & Bellon, G. (2013). Convective entrainment and Large-Scale organization of tropical precipitation: Sensitivity of the CNRM-CM5 hierarchy of models. *Journal of Climate*, *26*(9), 2931–2946.
Oueslati, B., & Bellon, G. (2015). The double ITCZ bias in CMIP5 models: Interaction between SST, large-scale circulation and precipitation. *Climate Dynamics*, *44*(3–4), 585–607.
Peatman, S. C., Methven, J., & Woolnough, S. J. (2018). Isolating the effects of moisture entrainment on convectively coupled equatorial waves in an aquaplanet GCM. *Journal of the Atmospheric Sciences*, *75*(9), 3139–3157.
Pike, A. C. (1971). Intertropical Convergence Zone studied with an interacting atmosphere and ocean model. *Monthly Weather Review*, *99*, 469–477.
Schneider, T. (2018). Feedback of atmosphere-ocean coupling on shifts of the Intertropical Convergence Zone. *Geophysical Research Letters*, *44*, 11,644–11,653. https://doi.org/10.1002/2017GL07581
Schneider, T., Bischoff, T., & Haug, G. H. (2014). Migrations and dynamics of the Intertropical Convergence Zone. *Nature*, *513*, 45–53.
Schott, F. A., McCreary Jr, J. P., & Johnson, G. C. (2004). Shallow overturning circulations of the tropical-subtropical oceans. *Earth's Climate*, *147*, 261–304.
Song, X., & Zhang, G. J. (2018). The roles of convection parameterization in the formation of double ITCZ syndrome in the NCAR CESM: I. Atmospheric processes. *Journal of Advances in Modeling Earth Systems*, *10*, 842–866. https://doi.org/10.1002/2017MS001191
Sperber, K. R., Annamalai, H., Kang, I.-S., Kitoh, A., Moise, A., Turner, A., et al. (2013). The Asian summer monsoon: An intercomparison of CMIP5 vs. CMIP3 simulations of the late 20th century. *Climate Dynamics*, *41*(9–10), 2711–2744.
Talib, J., Woolnough, S. J., Klingaman, N. P., & Holloway, C. E. (2018). The role of the cloud radiative effect in the sensitivity of the Intertropical Convergence Zone to convective mixing. *Journal of Climate*, *31*(17), 6821–6838. https://doi.org/10.1175/JCLI-D-17-0794.1
Terray, L. (1998). Sensitivity of climate drift to atmospheric physical parameterizations in a coupled Ocean-Atmosphere general circulation model. *Journal of Climate*, *11*, 1633–1658.
Tian, B., & Dong, X. (2020). The double-ITCZ bias in CMIP3, CMIP5 and CMIP6 models based on annual mean precipitation. *Geophysical Research Letters*, *47*, e2020GL087232. https://doi.org/10.1029/2020GL087232
Tomas, R. A., Deser, C., & Sun, L. (2016). The role of ocean heat transport in the global climate response to projected Arctic sea ice loss. *Journal of Climate*, *29*(19), 6841–6859.
Valcke, S., Craig, T., & Coquart, L. (2013). OASIS3 user guide (*TR/CMGC/13/17*): CERFACS (Centre Européen de Recherche et de Formation Avancée en Calcul Scientifique).
Voigt, A., Biasutti, M., Scheff, J., Bader, J. A., Bordoni, S., Codron, F., et al. (2016). The tropical rain belts with an annual cycle and a continent model intercomparison project: TRACMIP. *Journal of Advances in Modeling Earth Systems*, *8*, 1868–1891. https://doi.org/10.1002/2016MS000748
Voigt, A., & Shaw, T. A. (2015). Circulation response to warming shaped by radiative changes of clouds and water vapour. *Nature Geoscience*, *8*(2), 102–106.
Wang, Y., Zhou, L., & Hamilton, K. (2007). Effect of convective entrainment/detrainment on the simulation of the tropical precipitation diurnal cycle. *Monthly Weather Review*, *135*(2), 567–585.
Wei, H.-H., & Bordoni, S. (2018). Energetic constraints on the ITCZ position in idealized simulations with a seasonal cycle. *Journal of Advances in Modeling Earth Systems*, *10*, 1708–1725. https://doi.org/10.1029/2018MS001313
Xiang, B., Zhao, M., Held, I. M., & Golaz, J.-C. (2017). Predicting the severity of spurious "double ITCZ" problem in CMIP5 coupled models from AMIP simulations. *Geophysical Research Letters*, *44*, 1520–1527. https://doi.org/10.1002/2016GL071992
Xiang, B., Zhao, M., Ming, Y., Yu, W., & Kang, S. M. (2018). Contrasting impacts of radiative forcing in the Southern Ocean versus southern tropics on ITCZ position and energy transport in one GFDL climate model. *Journal of Climate*, *31*(14), 5609–5628.
Zhang, G. J., & Wang, H. (2006). Toward mitigating the double ITCZ problem in NCAR CCSM3. *Geophysical Research Letters*, *33*, L06709. https://doi.org/10.1029/2005GL025229